

# Liver cancer development driven by the AP-1/c-Jun~Fra-2 dimer through c-Myc (Author copy)

Latifa Bakiri<sup>1</sup>

<sup>1</sup>Affiliation not available

April 25, 2024

Latifa Bakiri<sup>1,2,\*</sup>, Sebastian C. Hasenfuss<sup>2,§</sup>, Ana Guío-Carrión<sup>2,#</sup>, Martin K. Thomsen<sup>3</sup>, Peter Hasselblatt<sup>4</sup> and Erwin F. Wagner<sup>1, 5,\*</sup>

<sup>1</sup> Laboratory Genes and Disease, Department of Laboratory Medicine, Medical University of Vienna (MUW), Vienna, Austria.

<sup>2</sup> Genes, Development and Disease Group, CNIO - National Cancer Research Centre, Madrid, Spain.

<sup>3</sup> Department of Biomedicine, University of Aarhus, Denmark.

<sup>4</sup> Department of Medicine II, University Hospital and Faculty of Medicine, Freiburg, Germany.

<sup>5</sup> Laboratory Genes and Disease, Department of Dermatology, Medical University of Vienna (MUW), Vienna, Austria.

<sup>§</sup> Current address: Beam Therapeutics, Cambridge, Massachusetts, USA.

<sup>#</sup> Current address: CNIC - National Center for Cardiovascular Research, Madrid, Spain.

\* Corresponding authors: Latifa Bakiri & Erwin F. Wagner, Department of Laboratory Medicine and Department of Dermatology, Medical University of Vienna, Lazarettgasse 14, A-1090 Vienna, Austria.

Tel: +43-1-40400-73506.

e-mail: erwin.wagner@meduniwien.ac.at, latifa.bakiri@meduniwien.ac.at

Running title: c-Jun/Fra-2 dimers in liver cancer

This is a prefinal, unformatted **author copy** of a manuscript published in PNAS: PMID: 38657045 / <https://doi.org/10.1073/pnas.2404188121>

**Keywords** : c-Jun/Fra-2, AP-1, HCC, mouse models, c-Myc

## Abstract

Hepatocellular carcinoma (HCC) is a leading cause of cancer-related death. HCC incidence is on the rise, while treatment options remain limited. Thus, a better understanding of the molecular pathways involved in HCC development has become a priority to guide future therapies. While previous studies implicated the AP-1 (Fos/Jun) transcription factor family members c-Fos and c-Jun in HCC formation, the contribution of Fos-related antigens 1 and 2 (Fra-1/2) is unknown. Here we show that hepatocyte-restricted expression of a single chain c-Jun~Fra-2 protein, which functionally mimics the c-Jun/Fra-2 AP-1 dimer, results in spontaneous HCC formation in c-Jun~Fra-2<sup>hep</sup> mice. Several hallmarks of human HCC, such as cell cycle dysregulation and the expression of HCC markers are observed in liver tumors arising in c-Jun~Fra-2<sup>hep</sup> mice. Tumorigenesis occurs in the context of mild inflammation, low-grade fibrosis and Ppar $\gamma$ -driven dyslipidemia.

Subsequent analyses revealed increased expression of c-Myc, evidently under direct regulation by AP-1 through a conserved distal 3' enhancer. Importantly, c-Jun<sup>+</sup>Fra-2-induced tumors revert upon switching off transgene expression, suggesting oncogene addiction to the c-Jun<sup>+</sup>Fra-2 transgene. Tumors escaping reversion maintained c-Myc and c-Myc target gene expression, likely due to increased c-Fos. Interfering with c-Myc in established tumors using the BET bromodomain inhibitor JQ-1 diminished liver tumor growth in c-Jun<sup>+</sup>Fra-2 mutant mice. Thus, our data establish c-Jun<sup>+</sup>Fra-2<sup>hep</sup> mice as a novel model to study liver tumorigenesis and identify the c-Jun/Fra-2-Myc interaction as a potential target to improve HCC patient stratification and/or therapy.

## Significance

Hepatocellular carcinoma (HCC) is a deadly cancer with limited treatment options. The AP-1 transcription factor components c-Fos and c-Jun were previously linked to HCC, but the role of Fra proteins was unclear. This study establishes a new mouse model for HCC research and reveals that hepatic expression of a c-Jun/Fra-2 dimer induces spontaneous tumors with HCC features. Tumor growth is fueled by dysregulated cell cycle, inflammation, dyslipidemia and increased c-Myc. Switching off c-Jun<sup>+</sup>Fra-2 reverts tumor growth, whereas escaping tumors maintain c-Myc, consistent with c-Jun/Fra-2-mediated regulation of c-Myc driving HCC. Furthermore, blocking c-Myc using the BET inhibitor JQ-1 halts tumor growth. The data suggest that the novel c-Jun/Fra-2-Myc interaction is pertinent to future clinical studies aimed at improving HCC patient care.

## Introduction

Primary liver cancer is the 6<sup>th</sup> most commonly diagnosed cancer and the 3<sup>rd</sup> leading cause of cancer death worldwide. Incidence and mortality are higher among men and in low to moderate income countries (1). Hepatocellular carcinoma (HCC), accounting for 75–85% of primary liver cancers, develops in the context of chronic liver diseases, such as hepatitis and/or metabolic dysfunction. HCC is increasingly associated with obesity, insulin resistance and the metabolic syndrome and has limited therapeutic options (2, 3). The signalling pathways most frequently involved in hepatocarcinogenesis include Wnt/ $\beta$ -catenin, mTOR, IL-6, TGF- $\beta$ , Ras, Rb, HGF/c-Met, and IGF1, which converge and modulate the activity of the NF- $\kappa$ B, p53, Stat3, c-Myc and AP-1 transcription factors (4-6).

The Jun (c-Jun, JunB, JunD) and Fos (c-Fos, FosB, Fra-1, Fra-2) proteins are components of the dimeric Activator Protein-1 (AP-1) transcription factor complex (7). While Jun proteins can form homo- or heterodimers, Fos proteins can only form heterodimers with a Jun protein. The AP-1 dimer combinations that co-exist in a given cell/biological context, together with dimer-specific variation in DNA sequence affinity and/or co-activator/repressor recruitment, determine the target genes that are positively or negatively regulated by AP-1. The AP-1 dimer pool is modulated by various signals, such as growth factors, inflammatory cytokines, mechanical and oxidative stress, and plays important roles in many diseases including cancer (7, 8). In genetically engineered mouse models (GEMMs), liver-specific inactivation of c-Jun revealed its essential role in liver regeneration (9), steatohepatitis (10), hepatocyte survival during acute hepatitis (11), endoplasmic reticulum (ER) stress (12), and liver cancer (13-18). In HCC, c-Jun promotes the survival of diethylnitrosamine (DEN)-induced pre-neoplastic hepatocytes by repressing c-Fos expression (16), while c-Fos is needed for DEN-induced hepatocarcinogenesis when the *c-jun* gene is intact (19). Furthermore, doxycycline (Dox)-switchable c-Fos expression in adult hepatocytes (c-Fos<sup>hep</sup>) leads to reversible liver inflammation, accumulation of toxic oxysterols and bile acids, activation of the DNA damage response (DDR), premalignant transformation and enhanced DEN-induced HCC (19). The hepatic functions of the other Jun and Fos proteins are less studied, especially in cancer. Hepatocyte-specific JunB inactivation increases liver damage during acute hepatitis, an effect that is largely counteracted by the pro-inflammatory role of JunB in hepatic NK/NKT cells (20). JunD knock-out mice are protected from chemically-induced liver fibrosis (21) and high fat diet (HFD)-induced hepatosteatosis (22). On the other hand, loss of Fra-1 sensitizes, while hepatic Fra-1, but not Fra-2, expression protects from acetaminophen-induced liver damage, an acute liver failure paradigm (23). Interestingly, Fra-1 and Fra-2 play redundant functions in hepatic lipid metabolism: Fra-1 or Fra-2 expression in hepatocytes prevented and could even revert HFD-induced hepatosteatosis by

suppressing the transcription of the nuclear receptor PPAR $\gamma$ , a central regulator of lipid metabolism, while single inactivation of either of the two genes had no effect (22, 24). In contrast, c-Fos activated hepatic *Pparg* transcription, while it suppressed another nuclear receptor LXR $\alpha$ , responsible for increased hepatic cholesterol and oxysterols (19, 22). Thus, Fra-1/2- and c-Fos-containing AP-1 dimers exert antagonistic effects on the *pparg2* promoter and lipid handling in the liver. When selected Jun and Fos monomers were tethered by a flexible polypeptide to force specific AP-1 pairing in a “single-chain” approach (25), and expressed in Dox-switchable AP-1<sup>hep</sup> mice, c-Jun $\sim$ Fra-2 dimers inhibited, whereas c-Jun $\sim$ c-Fos, JunB $\sim$ c-Fos, and JunD $\sim$ c-Fos dimers activated PPAR $\gamma$  expression and signalling (22, 24).

In this study, we show that hepatic expression of c-Jun $\sim$ Fra-2 dimers results in spontaneous and reversible HCC formation, while mice expressing Fra-1/2 monomers or c-Jun $\sim$ Fra-1 dimers remained tumor-free. c-Jun $\sim$ Fra-2 dimers promote tumorigenesis in murine and human liver cells, in significant part through direct transcriptional activation of *c-myc* expression. Furthermore, we show that established tumors are largely addicted to c-Jun $\sim$ Fra-2 and sensitive to JQ-1, a BET bromodomain inhibitor that inhibits c-Myc activity.

## Results

### Spontaneous liver tumors in c-Jun $\sim$ Fra-2<sup>hep</sup> mice

Jun $\sim$ Fra-2<sup>hep</sup> mice had a shorter lifespan compared to controls, with a median survival of 45 weeks after switching on the transgene (Suppl. Figure 1A). Mutant and control littermates were sacrificed at different time points after transgene induction, which was always started at weaning by Doxycycline (Dox) removal. All time points indicated hereafter are post-transgene induction. Macroscopically visible liver tumors were observed at 9 months (Figure 1A), while increased liver to body weight ratio was already apparent at 2 months (Suppl. Figure 1B). Nodule number and size was variable (Suppl. Figure 1C), but the phenotype was highly penetrant, with almost 90% of Jun $\sim$ Fra-2<sup>hep</sup> mice having at least one macroscopically visible tumor nodule at 9 months (Suppl. Figure 1D). Notably, Fra-1<sup>hep</sup>, Fra-2<sup>hep</sup> and Jun $\sim$ Fra-1<sup>hep</sup> mice expressing Fra-1/2 monomers (23) or Jun $\sim$ Fra-1 dimers, generated with a similar strategy (see methods and Suppl. Figure 7) and kept up to 15 months off Dox never or rarely developed liver tumors (Suppl. Figure 1D). Histologically, hyperplastic nodules, adenoma and HCC were identified in Jun $\sim$ Fra-2<sup>hep</sup> liver sections (Figure 1A), while the HCC biomarker (26) ‘Protein-induced-by-vitamin-K-absence-or-antagonist-II’ (PIVKA), was increased in Jun $\sim$ Fra-2<sup>hep</sup> sera at 9 months (Figure 1B). Alpha-fetoprotein (AFP), a more commonly used HCC biomarker, was elevated in the serum of Jun $\sim$ Fra-2<sup>hep</sup> mice as early as 1 month (Figure 1C), but not in aged Fra-1<sup>hep</sup>, Fra-2<sup>hep</sup> or Jun $\sim$ Fra-1<sup>hep</sup> mice (Suppl. Figure 1E). AFP was also detected by IHC in Jun $\sim$ Fra-2<sup>hep</sup> liver tumors (Figure 1D). IHC-positivity for ‘minichromosome-maintenance-complex-component-2’ (Mcm2) and Sox9, which have been associated with HCC development and Sorafenib resistance (27-29), was also observed in the tumors (Figure 1D). Hypoalbuminemia (Suppl. Figure 1F), increased alanine (ALT) and aspartate (AST) aminotransferases as well as alkaline phosphatase (ALP) (Suppl. Figure 1G) were also observed in Jun $\sim$ Fra-2<sup>hep</sup> mice, consistent with early onset liver dysfunction and damage.

Macroscopically visible liver tumors were dissected from Jun $\sim$ Fra-2<sup>hep</sup> mice at 9 months, together with small liver pieces from areas that appeared macroscopically tumor-free, hereafter termed ‘non-tumoral’ (NT), and compared to livers of control littermates by RNA and protein analyses. Quantitative reverse transcription-PCR (qRT-PCR) revealed increased mRNA expression of oncofetal (*h19*, *nope*, *dlk1*, *bex1*), cancer cell stemness (*cd133*, *cd44*, *sox9*), HCC (mcm2, gp73, ly6d) and replicative senescence (p16) markers in Jun $\sim$ Fra-2<sup>hep</sup> tumors and non-tumoral (NT) areas (Figure 1E). Increased Gp73 and Bex was confirmed by immunoblotting (Figure 1F). Activation of endoplasmic reticulum (ER) stress with increased PERK and eIF2a phosphorylation and Bip protein expression was also evident in Jun $\sim$ Fra-2<sup>hep</sup> tumoral and non-tumoral extracts compared to control livers (Suppl. Figure 1H). Increased p53, p21 and S139-phosphorylation of histone H2AX ( $\gamma$ H2AX), a surrogate marker of DNA damage, as well as decreased p19 were consistent with aberrant cell cycle and replicative stress (Figure 1G, Suppl. Figure 1I). Overall, most of the molecular changes observed in the tumors were also seen in the non-tumoral areas indicating that these areas are likely pre-neoplastic. Consistently, p21- and  $\gamma$ H2AX-positive hepatocytes and increased *p21*, *p16* and *p53* mRNA were already apparent in the livers of Jun $\sim$ Fra-2<sup>hep</sup> mice at 2 months (Figure 1H, Suppl. Figure 1I-J).

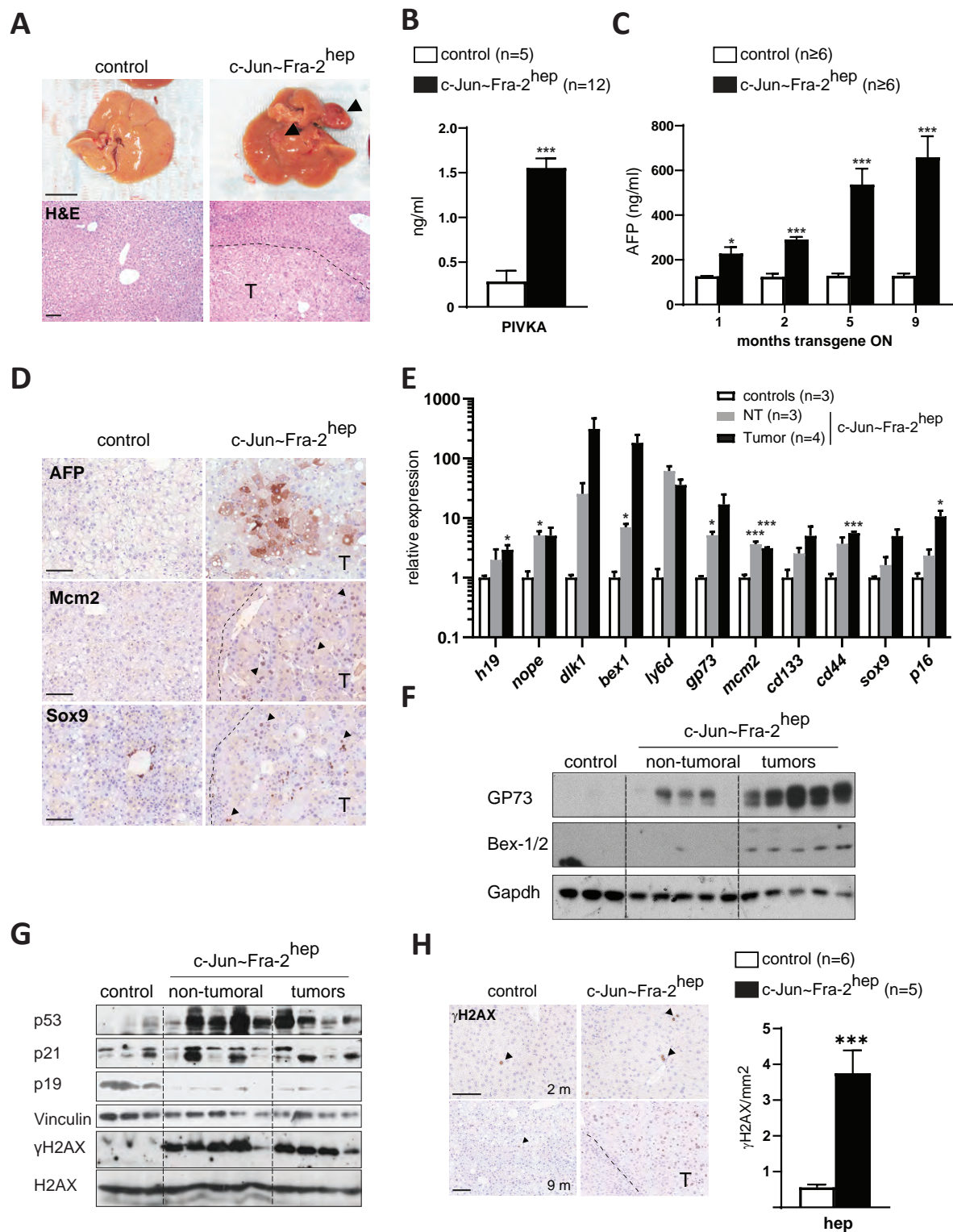


Figure 1. Bakiri et al.

**Figure 1: Liver tumors in c-Jun~Fra-2<sup>hep</sup> mice.** **A.** Liver morphology and histology in a c-Jun~Fra-2<sup>hep</sup> and representative control mouse. Bar = 1 cm (top) and 100μm (H&E, bottom), tumors (T) are indicated by arrows and dotted line. **B.** Serum protein induced by vitamin K absence or antagonist-II (PIVKA), also known as des-gamma-carboxy-prothrombin (DCP). **C.** Serum alpha-fetoprotein (AFP) in c-Jun~Fra-2<sup>hep</sup> mice and littermate controls over time. **D.** AFP, Mcm2 and Sox9 immunohistochemistry (IHC) in

## Enhanced proliferation and moderate inflammation in $c\text{-Jun}^{\sim}\text{Fra-2}^{\text{hep}}$ livers

Genome-wide transcription profiling by RNAseq was performed on 2- and 9-month liver samples. Unsupervised principal-component analysis (PCA) clearly separated the samples along PC1 and PC2 according to genotype and age, respectively (Figure 2A). Interestingly, while tumoral samples also separated from non-tumoral (NT) along PC2, the two tumors isolated from the same mouse appeared more distant from each-other than the two tumors isolated from different mice, consistent with inter-tumoral heterogeneity (Figure 2A). Gene set enrichment analysis (GSEA (30)) revealed enrichment in MSigDB Hallmarks gene sets related to cell cycle, p53 pathway, cell death and hypoxia in the 3 mutant groups, when compared to their respective control littermates (Suppl. Figure 2A). CIBERSORTx (31) computational deconvolution at 2 months using a murine hepatocyte matrix (32) indicated perturbed liver zonation, with increased Zone 2 and undetectable Zone 3 hepatocytes (Suppl. Figure 2B), which was confirmed by diffuse peri-central Glutamine synthetase IHC positivity in mutants (Suppl. Figure 2C). The mean expression profile of the 4 tumors relative to control livers was next compared by GSEA with a collection of human and murine liver cancer signatures. A significant correlation was observed with HCC gene signatures, in particular those associated with poor outcome, such as Hoshida subclass S1 (33), Boyault subclass G3 (34), Woo cancer recurrence (35), the hepatoblast subtype of human HCC with prominent AP-1 (36) and paediatric hepatoblastoma with upregulated Myc signalling (37) (Figure 2B). These gene signatures are all characteristic of dedifferentiation, fetal liver-like gene expression, high proliferation, and aggressiveness. There was also a good correlation with murine liver cancer signatures (38), in particular those arising in mice expressing a Myc transgene (Figure 2B). Increased proliferation and altered cell cycle was confirmed by Ki67 and Cyclin D1 IHC (Figure 2C-D) as well as immunoblot and qRT-PCR for a panel of cyclins and Cdks (Suppl. Figure 2D-E). Increased Cyclin A is consistent with *ccna2* (encoding Cyclin A2) being a direct target of the  $c\text{-Jun}/\text{Fra-2}$  dimer in cultured cells (25). Increased Ki67-positivity was also observed in non-parenchymal, likely immune cells as early as 2 months (Figure 2D), along with increased interleukin 6 (*il6*) mRNA (Suppl. Figure 2E). Therefore, the immune and inflammatory profile of  $\text{Jun}^{\sim}\text{Fra-2}^{\text{hep}}$  livers was examined in more detail. A moderate but consistent increase in immune cell-related marker expression was observed by IHC (Figure 2E, Suppl. Figure 2F) and qRT-PCR (Figure 2F, Suppl. Figure 2G). Furthermore, GSEA using human MSigDB C8 liver cell gene sets (39) revealed that Kupffer cell signatures were among the top enriched in mutant  $\text{Jun}^{\sim}\text{Fra-2}^{\text{hep}}$  livers (Suppl. Figure 2H). Elevated myeloid cell abundance in mutant livers was confirmed by CIBERSORTx deconvolution using a murine matrix (32), and TREM2-positive macrophages, that are high in HCC and associate with poor prognosis (40) were notably increased (Figure 2G).

We next evaluated signalling pathways that could connect inflammation and proliferation. The relative phosphorylation of ERK, JNK and p38 was not noticeably changed at 9 months, while PTEN, AKT and GSK3 $\beta$  phosphorylation was increased to variable extents (Suppl. Figure 2I). The MSigDB Hallmarks gene sets: Inflammatory response, TNF/NF- $\kappa$ B and IL6/JAK/STAT3 were enriched in the  $\text{Jun}^{\sim}\text{Fra-2}^{\text{hep}}$  mutant groups (Figure 2H). This is in line with increased relative STAT3 phosphorylation and increased p-STAT3-positive cells at 2 and 9 months, although the phosphorylation of the p65 NF- $\kappa$ B subunit was not changed (Figure 2I, Suppl. Figure 2J-K). These results imply that hepatic  $\text{Jun}^{\sim}\text{Fra-2}$  expression leads to cellular and molecular characteristics of malignant transformation in a context of moderate inflammation, even before visible tumors are detected.

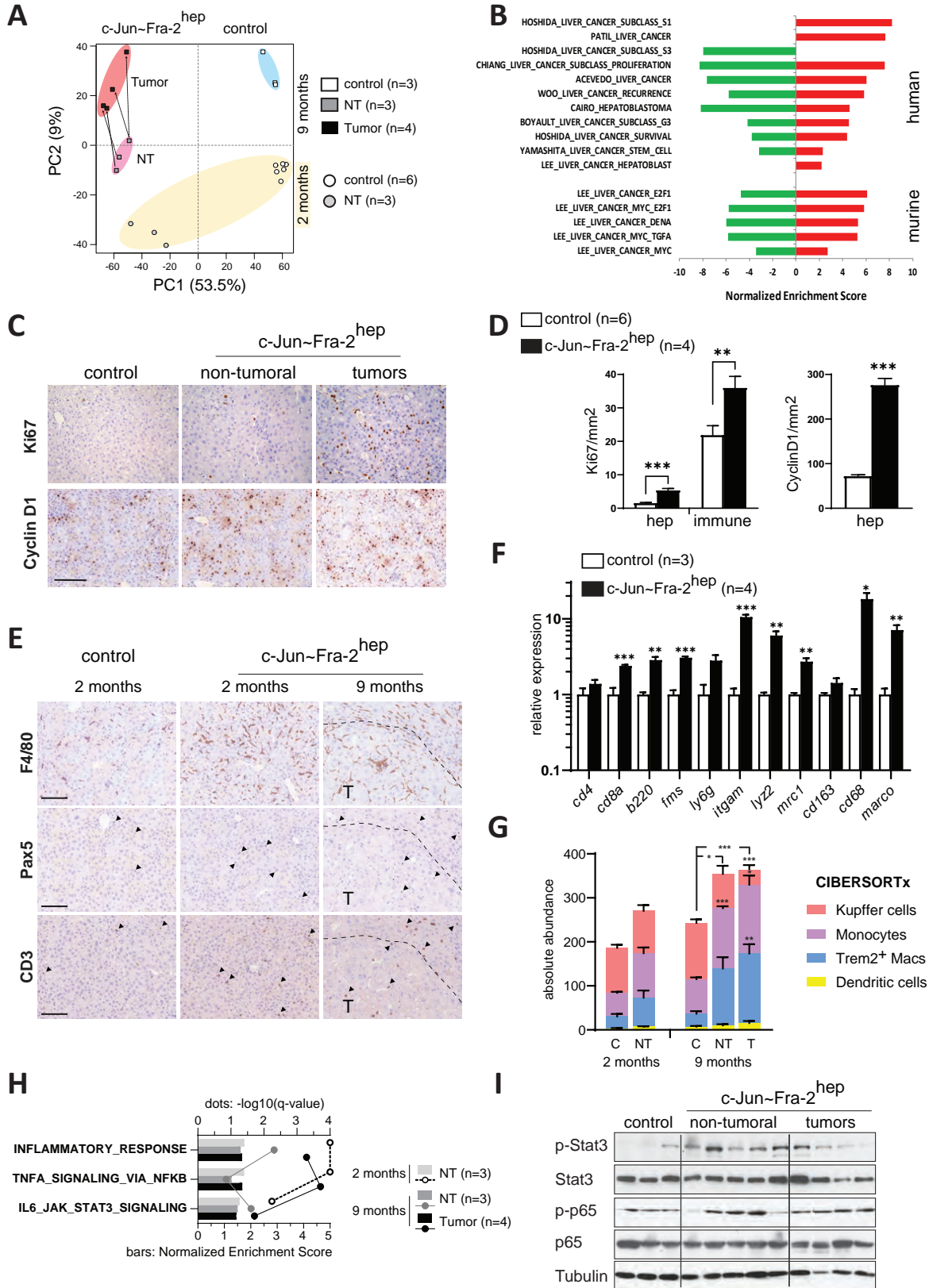


Figure 2. Bakiri et al.

Figure 2: **Phenotypic characterization and inflammation in *c-Jun~Fra-2*<sup>hep</sup> livers.** **A.** Principal component analysis (PCA) of RNAseq data. PC1 and PC2 account for 62.5% of sample variability. Individual samples from 2 and 9 months of transgene expression are depicted with circles and squares, respectively and the correspondence between non-tumoral (NT) and tumoral samples from the same mouse indicated with dotted arrows. **B.** Normalized enrichment scores in *c-Jun~Fra-2*<sup>hep</sup> liver tumors relative to controls (RNAseq,

## Low-grade fibrosis and dyslipidemia in $c\text{-Jun}^{\sim}\text{Fra-2}^{\text{hep}}$ livers

Fibrosis and steatosis are often associated with HCC. At 2 months, Trichrome staining of liver sections (Figure 3A), qRT-PCR (Figure 3B) and WebGestalt (41) overrepresentation of matrix/collagen-related Reactome and Gene Ontology terms (Figure 3C), as well as enrichment in MSigDB C8 hepatic stellate cell signatures (Suppl. Figure 2H), supported the occurrence of fibrotic events in  $\text{Jun}^{\sim}\text{Fra-2}^{\text{hep}}$  mutant livers. Increased  $\text{TGF}\beta$  signalling was also apparent at 9 months with increased *tgfb2/tgfbR2* mRNA expression (Suppl. Figure 3A) and relative Smad2 phosphorylation (Figure 3D). On the other hand, while the epithelial-to-mesenchymal transition MSigDB hallmark gene set was enriched in mutant datasets, lipid/peroxisome metabolism-related hallmarks had negative enrichment scores (Suppl. Figure 3B), consistent with decreased Oil Red O staining and Pparg positivity in liver sections (Figure 3E). This is in line with the suppression of Pparg signalling and high fat diet-induced NAFLD in  $c\text{-Jun}^{\sim}\text{Fra-2}^{\text{hep}}$  mice (22). Decreased protein and mRNA expression of Pparg and Pparg targets were apparent at 2 and 9 months (Figure 3F, Suppl. Figure 3C-D). LXR and LXR signalling, driving early pre-neoplastic events in Fos-expressing mice (19), were not consistently affected in  $c\text{-Jun}^{\sim}\text{Fra-2}^{\text{hep}}$  mice (Suppl. Figure 3E). Liver triglycerides (Figure 3G), serum triglycerides and cholesterol (Suppl. Figure 3F) were also decreased in mutant mice at 9 months, similar to what was observed after high fat diet (22). These data indicate that while low-grade fibrosis might contribute to liver cancer development in  $\text{Jun}^{\sim}\text{Fra-2}^{\text{hep}}$  mice, tumors occur in a dyslipidemic context with decreased hepatic lipids.

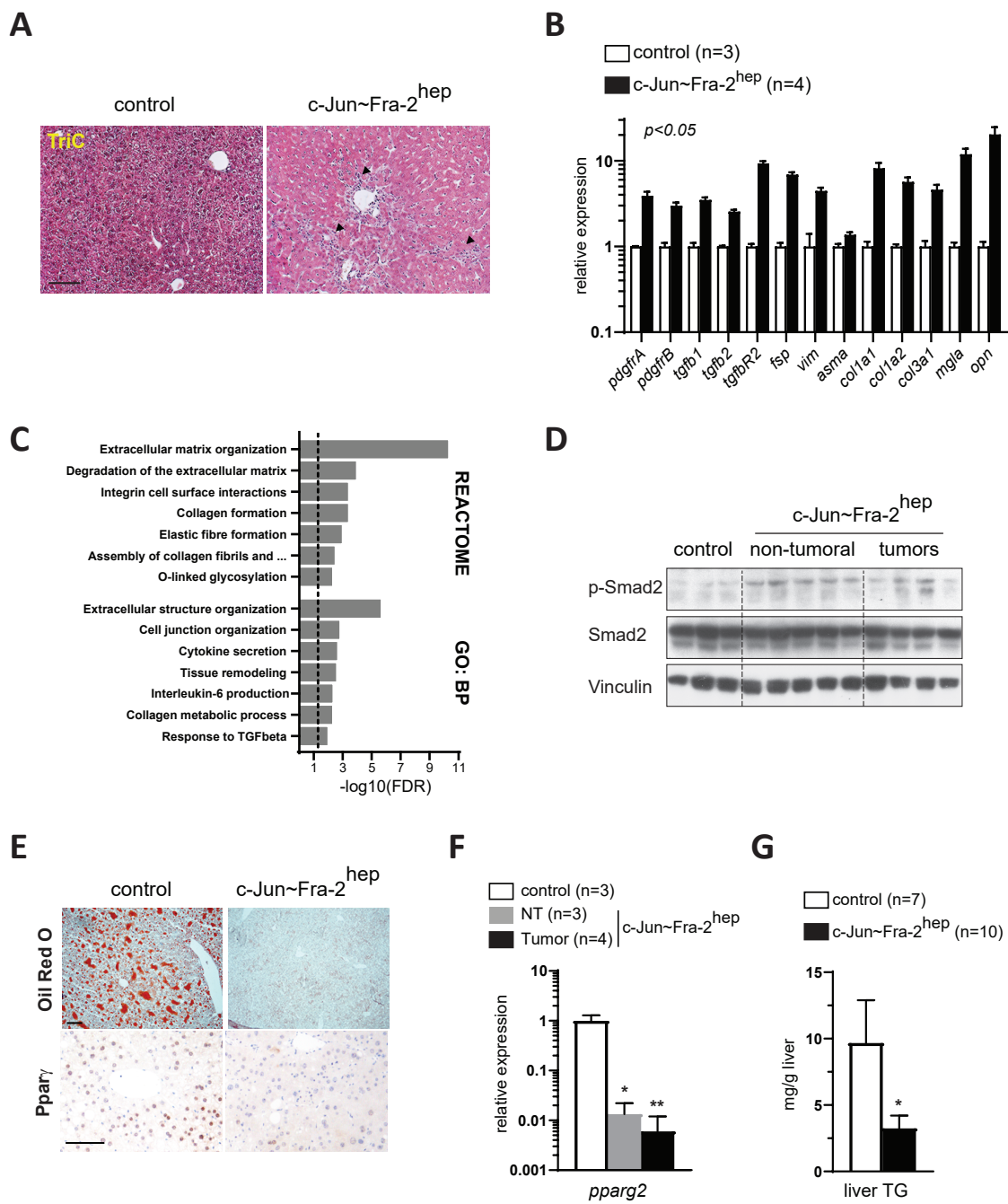


Figure 3. Bakiri et al.

**Figure 3: Fibrosis and lipid metabolism in  $c\text{-Jun}^{\sim}\text{Fra-2}^{\text{hep}}$  livers.** **A.** Masson Trichrome staining of  $c\text{-Jun}^{\sim}\text{Fra-2}^{\text{hep}}$  and control liver sections at 2 months. Bar = 100  $\mu\text{m}$ , arrows point to fibrotic areas. **B.** qRT-PCR quantification of fibrosis-associated genes in  $c\text{-Jun}^{\sim}\text{Fra-2}^{\text{hep}}$  livers compared to controls at 2 months,  $p < 0.05$  for each mRNA. **C.** Overrepresentation analysis (ORA, WebGestalt) of upregulated genes  $c\text{-Jun}^{\sim}\text{Fra-2}^{\text{hep}}$  livers at 2 months (RNAseq,  $n = 6$  controls and 3 mutants) using Pathways/Reactome (enrichment

### c-Jun<sup>+</sup>Fra-2 binds a *c-myc* 3' enhancer and increases c-Myc and Myc target gene expression

c-Myc is central to HCC pathogenesis and is connected to the IL6/JAK/Stat3 and PI3K/AKT/GSK3 $\beta$  pathways (42, 43). Consistent with the prominent enrichment in Myc-related murine and human liver cancer signatures (Figure 2B) and the increased IL6/JAK/Stat3 and PI3K/AKT/GSK3 $\beta$  pathway activities (Figure 2H-I, Suppl. Figure 2I-K), c-Myc protein expression was increased in c-Jun<sup>+</sup>Fra-2<sup>hep</sup> livers at 2 and 9 months (Figure 4A, Suppl. Figure 4A). *c-myc* mRNA was also increased at 2 months, but not in age-matched Jun<sup>+</sup>Fra-1<sup>hep</sup> or Fra<sup>hep</sup> mice (Suppl. Figure 4B). *foxm1*, an HCC-relevant protein often connected to Myc (44), was also increased (Suppl. Figure 4C), along with a panel of c-Myc target genes (Figure 4B).

A 3' enhancer, 1.4 kb downstream of the MYC transcriptional stop, is bound and activated by JUN-containing dimers in human colorectal cancer cells, cooperatively with  $\beta$ -catenin/TCF4 (45). This Wnt-responsive enhancer (WRE) is conserved in the mouse, including the AP-1 consensus motif TGACTCA, and a similar motif was identified in the *c-myc* promoter (Figure 4C). Chromatin immunoprecipitation using hepatic chromatin from c-Jun<sup>+</sup>Fra-2<sup>hep</sup> mice at 2 months and Fra-2 (Figure 4D) or Flag (Figure 4E-F) antibodies followed by quantitative PCR (ChIP-qPCR) revealed that c-Jun<sup>+</sup>Fra-2 efficiently bound the *c-myc* -WRE and the AP-1-responsive Dusp1 promoter used as a positive control, but not the *c-myc* promoter. The enrichment in WRE ChIP-qPCR fragments was negligible, when hepatic chromatin from Fra-2<sup>hep</sup> mice was employed (Figure 4F), consistent with unaltered *c-myc* expression in these samples (Suppl. Figure 4B). Transient transfection experiments using the murine AML12 liver cell line revealed that c-Jun<sup>+</sup>Fra-2 expression increased endogenous *c-myc* mRNA along with the activity of a *c-myc* -WRE luciferase reporter, while Fra-2 had little to no effect (Figure 4G).

*c-myc* expression was next evaluated in experimental HCC models with Fra-2 or c-Jun deficiency. Hepatic *c-myc* and *c-jun* expression was unchanged upon injection of the chemical carcinogen diethylnitrosamine (DEN) to adult Fra-2 <sup>$\Delta^{\lambda}$</sup>  mice lacking Fra-2 in hepatocytes (Suppl. Figure 4D). Furthermore, DEN-induced tumorigenesis was similar between Fra-2 <sup>$\Delta^{\lambda}$</sup>  and Fra-2-proficient littermates, as were serum AFP and ALT (Suppl. Figure 4E, F) and *c-myc* and *c-jun* expression in isolated tumors (Suppl. Figure 4G). Mice lacking hepatic c-Jun are resistant to experimental HCC paradigms (13, 15, 17, 18) and a significant reduction in *c-myc* mRNA (Figure 4H) and protein (Figure 4I) expression are observed in c-Jun <sup>$\Delta^{\lambda}$</sup>  livers during HBV-driven tumorigenesis (18). These data indicate that Fra-2 is dispensable, while c-Jun is needed to modulate c-myc expression, at least in the context of DEN- and HBV-induced tumorigenesis, respectively.

We next explored the connection between JUN, FRA2 and MYC in human liver cancer. Datamining of genome-wide ChIPseq of HepG2 hepatoma cells (46) revealed JUN- and FRA2- ChIP peaks in a transcriptionally active genomic area consistent with the MYC WRE (Suppl. Figure 4H). Furthermore, *MYC* mRNA expression was abrogated in HepG2 cells upon CRISPR/cas9 deletion of the MYC WRE, while it was increased after transient expression of c-Jun<sup>+</sup>Fra-2 in the parental cell line (Suppl. Figure 4I) and decreased upon siRNA knock-down of JUN or JUNB (Suppl. Figure 4J). HCC RNAseq data from treatment-naïve patients (TCGA-LIHC) generated by The Cancer Genome Atlas (47) were next explored. MYC expression, reported as the average number of 'Fragments Per Kilobase of exon per Million reads' (FPKM), correlated with each of JUN and FRA2 independently (Suppl. Figure 4K). Cohorts with high (HH) or low (LL) JUN and FRA2 expression were next defined, corresponding to 37% and 27% of the samples, respectively (Suppl. Figure 4K, right panel). Strikingly, MYC, FOXM1 and Cyclin D1 (CCND1) expression was found higher (Suppl. Figure 4L) and overall survival lower (Suppl. Figure 4M) in the HH group. Taken together these data indicate that the modulation of *c-myc* expression by c-Jun/Fra-2 is likely also occurring in human hepatocytes and could be relevant to HCC progression.

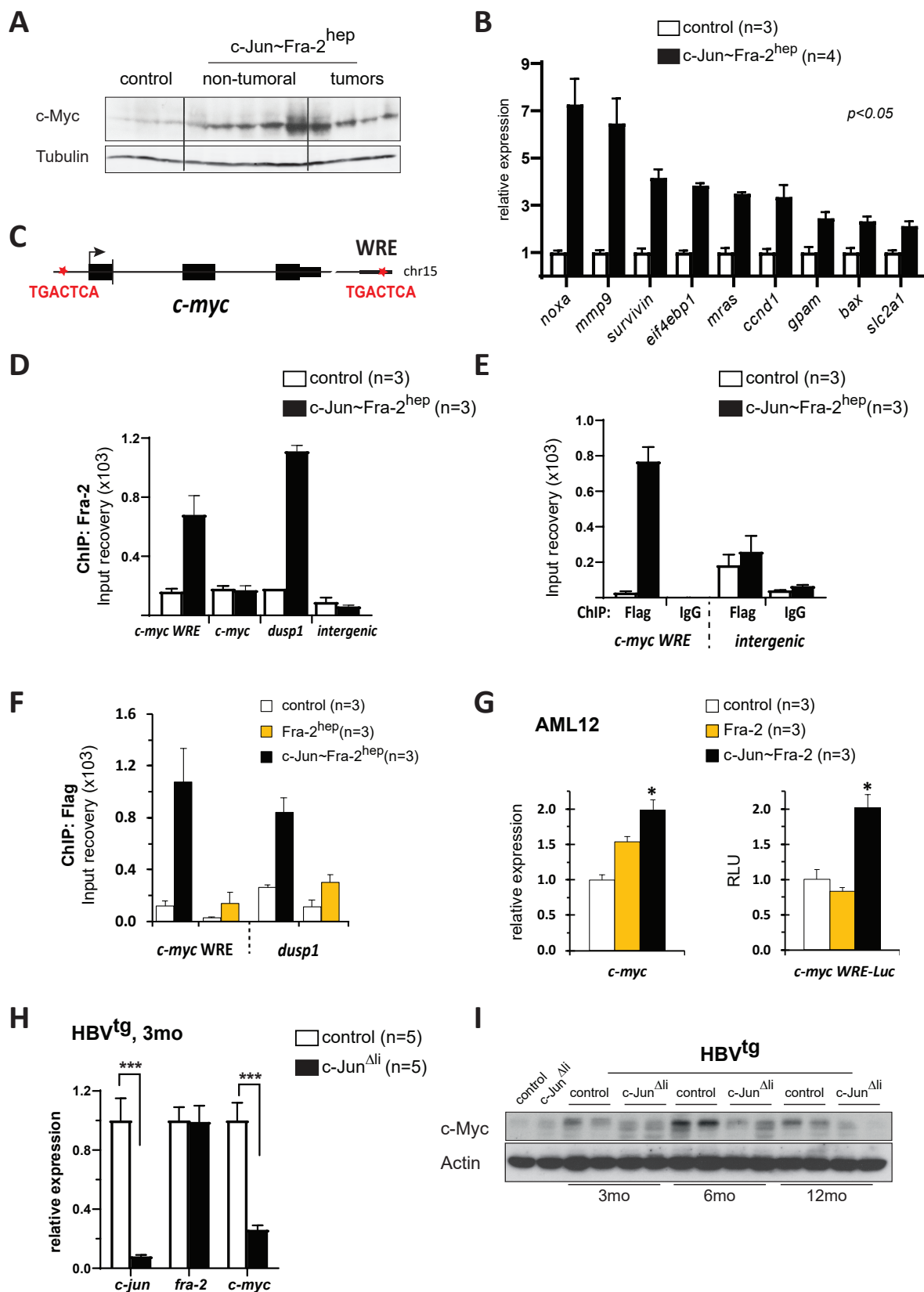


Figure 4. Bakiri et al.

Figure 4: Transcriptional control of c-Myc by c-Jun~Fra-2 in the liver. **A**. Immunoblot analyses of c-Myc in liver extracts from c-Jun~Fra-2<sup>hep</sup> mice (non-tumoral and tumors) and controls. **B**. qRT-PCR quantification of c-Myc target genes c-Jun~Fra-2<sup>hep</sup> livers at 2 months. *p* < 0.05 for each mRNA. **C**. Schematic

## c-Jun<sup>+</sup>Fra2<sup>hep</sup> tumors are reversible, but addicted to *c-myc* expression

We next investigated whether c-Jun<sup>+</sup>Fra-2 is necessary to maintain the tumor phenotype by utilizing the “tetracycline switch” in c-Jun<sup>+</sup>Fra-2<sup>hep</sup> mice. c-Jun<sup>+</sup>Fra-2 was induced for 9 months, and the mice subsequently put back on Dox to halt c-Jun<sup>+</sup>Fra-2 expression and sacrificed 6 months later (Figure 5A). At this OFF endpoint, approximately 2/3 of the c-Jun<sup>+</sup>Fra-2<sup>hep</sup> mice, hereafter termed “reverted”, had no visible liver nodule at necropsy, while the rest of the c-Jun<sup>+</sup>Fra-2<sup>hep</sup> mice, hereafter “escapers”, presented at least one visible surface nodule (Figure 5B). Liver to body weight ratio (Suppl. Figure 5A) and serum AFP (Figure 5C) were comparable to controls in the reverted mice, while half (liver/body) to most (AFP) escapers had higher values and were similar to c-Jun<sup>+</sup>Fra-2<sup>hep</sup> mice sacrificed after 9 months of c-Jun<sup>+</sup>Fra-2 expression (ON). Serum ALT at end point was more heterogeneous, but escapers were still in the higher ranges (Suppl. Figure 5A).

Six c-Jun<sup>+</sup>Fra-2<sup>hep</sup> mice, hereafter termed mutant-1 to -6, were next followed longitudinally by liver ultrasonography (US) and serum monitoring along the reversion protocol. These mice had 1 to 3 tumors of variable size and roughly similar AFP, ALT, and ALP values (Suppl. Table 1A). While all 6 c-Jun<sup>+</sup>Fra-2<sup>hep</sup> mice displayed a sharp drop in serum AFP, approaching control levels after 8 weeks, AFP increased again in mutant-5 and even more in mutant-6 (Suppl. Figure 5B). High ALT concentrations were also measured at end point in these 2 mice, whereas ALP was comparable to control values in all 6 c-Jun<sup>+</sup>Fra-2<sup>hep</sup> mice (Suppl. Table 1A). US monitoring revealed that the fate of the individual tumors was heterogeneous and rather independent of their initial size or mouse of origin (Figure 5D, Suppl. Table 1A). Some tumors regressed to very small (T3 in mutant-4 and T1 in mutant-6) or below detection limit (T1 and T2 in mutant-4, all tumors in mutant-1 and mutant -2), while other tumors initially regressed, but resumed growing after a variable period (T1 in mutant-5 and T2 in mutant-6). We also observed the emergence of new tumors, with different sizes, latencies and growth kinetics, such as T3\* in mutants 5 and 6 (Figure 5D, Suppl. Table 1A). Although we cannot rule out that these tumors were overlooked at start due to US limitations, it remains striking that the timing of the AFP “rebound” in mutants 5 and 6 roughly corresponds to the regrowth of pre-existing tumors and/or detection of new tumors in these mice (Figure 5D, Suppl. Figure 5B).

Liver tumors were next dissected from a group of escapers, together with non-tumoral (NT) areas and compared to (tumor-free) livers from reverted and control littermates, as well as non-tumoral and tumoral areas from mice sacrificed after 9 months of c-Jun<sup>+</sup>Fra-2 expression (ON). qRT-PCR for *fra-2* (Figure 5E) and *c-Jun<sup>+</sup>Fra-2* (Suppl. Figure 5C) confirmed that c-Jun<sup>+</sup>Fra-2 was barely detectable in the samples collected at the OFF endpoint. However, while *c-myc* mRNA was decreased to control levels in reverted livers and in escapers’ NT areas, escaping tumors had high *c-myc* expression (Figure 5F) and detectable c-Myc-positive cells by IHC (Suppl. Figure 5D). qRT-PCR analyses revealed high expression of oncofetal, cancer cell stemness, HCC and replicative senescence markers in escaping tumors (Figure 5G), as well as *foxm1*, *p21* and a panel of c-Myc target genes (Suppl. Figure 5E), while the corresponding NT areas displayed an expression profile more similar to controls (Figure 5G, Suppl. Figure 5E). These data are consistent with c-Myc being an essential molecular determinant of tumor formation and maintenance in c-Jun<sup>+</sup>Fra-2<sup>hep</sup> mice. Interestingly, some of the escaping tumors displayed increased Fos mRNA (Suppl. Figure 5F) and protein (Suppl. Figure 5D). As *c-myc* and c-Myc target gene expression is increased in the pre-neoplastic livers of Fos<sup>hep</sup> mice (Suppl. Figure 5G), Fos-containing AP-1 dimers likely substitute for c-Jun<sup>+</sup>Fra-2 to maintain *c-myc* expression, at least in a subset of escaping tumors.

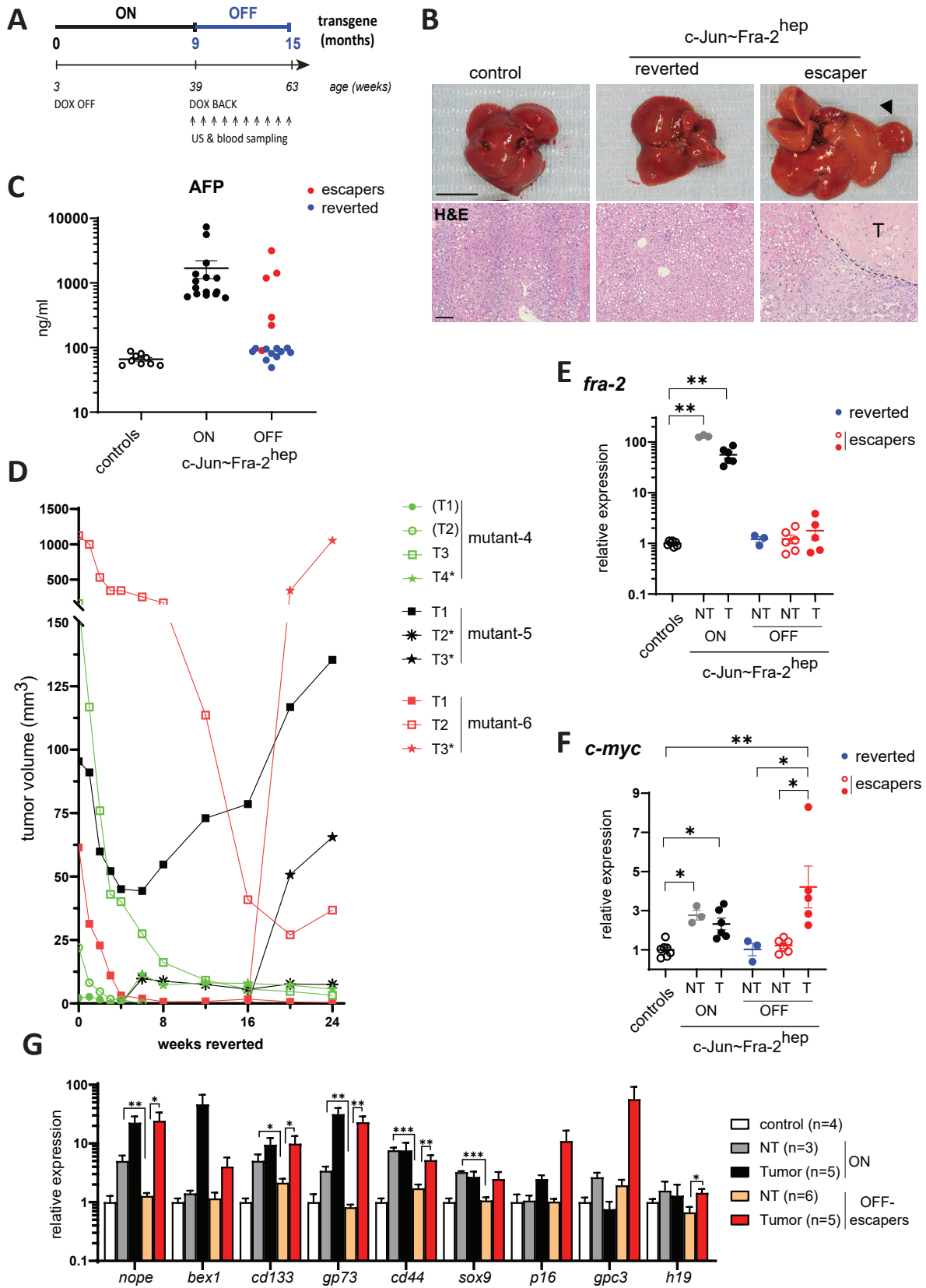


Figure 5. Bakiri et al.

Figure 5: Reversibility and oncogene addiction(s) of  $c\text{-Jun}^{\sim}\text{Fra-2}^{\text{hep}}$  liver tumors. **A**. Experimental design and timeline of the reversion experiment:  $c\text{-Jun}^{\sim}\text{Fra-2}^{\text{hep}}$  mutants with 9 months of transgene expression (off Dox at weaning) were put back on Dox, followed over time and compared to littermate controls

## Therapeutic value of a BET bromodomain inhibitor in c-Jun<sup>~</sup>Fra-2<sup>hep</sup> mice

The therapeutic potential of interfering pharmacologically with c-Myc expression and activity was tested in c-Jun<sup>~</sup>Fra-2<sup>hep</sup> mice employing JQ-1, a BET bromodomain inhibitor widely used in basic research (48, 49). When c-Jun<sup>~</sup>Fra-2 was induced for 2 months prior to 4 weeks of treatment (Suppl. Figure 6A), JQ-1 decreased hepatic c-Myc protein expression (Figure 6A), while c-Jun<sup>~</sup>Fra-2 was not affected (Figure 6A, Suppl. Figure 6B). Hepatic *c-myc* mRNA was unchanged, when comparing JQ-1- to vehicle-treated c-Jun<sup>~</sup>Fra-2<sup>hep</sup> mice, while mRNA expression of *foxm1*, *ccna2* and a panel of c-Myc target genes was decreased (Suppl. Figure 6C). Serum AFP, ALT and AST were ameliorated in JQ-1 treated c-Jun<sup>~</sup>Fra-2<sup>hep</sup> mice, while ALP remained high (Suppl. Figure 6D-E). Finally, Ki67, Cyclin D1 and  $\gamma$ H2AX indexes were reduced upon JQ1 treatment (Suppl. Figure 6F), consistent with a potential beneficial effect of JQ1 on the pre-neoplastic events occurring in c-Jun<sup>~</sup>Fra-2<sup>hep</sup> mice.

Next, 6 c-Jun<sup>~</sup>Fra-2<sup>hep</sup> mice were randomized at 9 months into 2 treatment groups and followed during 8 weeks to assess the effect of JQ1 on already established tumors (Suppl. Figure 6A). At end point necropsy, most JQ-1-treated c-Jun<sup>~</sup>Fra-2<sup>hep</sup> mice had smaller and fewer liver nodules compared to their vehicle-treated counterparts (Figure 6B). Serum AFP rapidly decreased in treated c-Jun<sup>~</sup>Fra-2<sup>hep</sup> mice and remained stable until end point, although slightly higher than controls (Figure 6C, Suppl. Table 1B). ALT and AST were still high at end point in JQ1-treated c-Jun<sup>~</sup>Fra-2<sup>hep</sup> mice, but unlike vehicle-treated counterparts, liver transaminases did not increase over time (Suppl. Figure 6G). In contrast, ALP slightly decreased, but remained comparable between treatment arms (Suppl. Figure 6G). Ultrasound follow up revealed that JQ-1 had a tumor-static effect: while tumors in vehicle-treated c-Jun<sup>~</sup>Fra-2<sup>hep</sup> mice increased in size over time, 6 out of 7 tumors in JQ-1-treated mice remained relatively stable and no new tumors were detected (Figure 6D, Suppl. Table 1B). qRT-PCR analyses comparing JQ-1-responsive to vehicle-treated tumors revealed decreased expression of *c-myc*, along with *foxm1* and other cell cycle- HCC-, immune- and fibrosis-related transcripts, while *c-Jun<sup>~</sup>Fra-2* was not affected (Figure 6E, Suppl. Figure 6H). Furthermore, we combined JQ1 with Sorafenib, a receptor tyrosine kinase inhibitor widely used to treat HCC. Sorafenib alone had no noticeable effect on tumor size after 8 weeks of treatment (Figure 6F), consistent with reports indicating Sorafenib resistance in HCC with high JUN/JNK (50, 51). JQ1 also slowed liver tumor growth in c-Jun<sup>~</sup>Fra-2<sup>hep</sup> mice treated with when co-administered with Sorafenib (Figure 6F) and reduced circulating AFP and ALT at endpoint (Figure 6G). Taken together, these results indicate that BET bromodomain inhibitors should be considered for HCC therapy, particularly in patients with high AP-1/Myc expression.

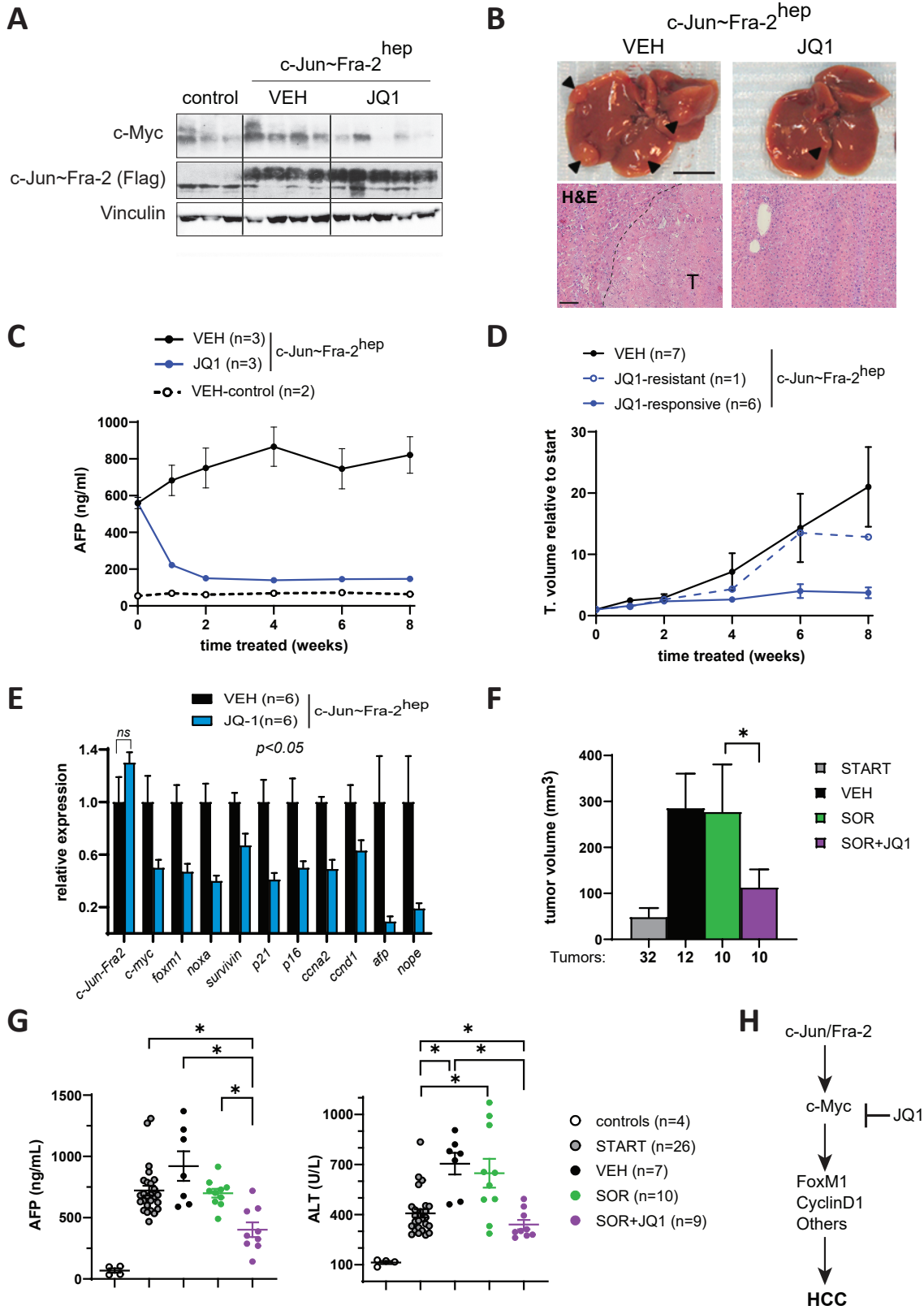


Figure 6. Bakiri et al.

Figure 6: **Therapeutic interventions in c-Jun~Fra-2<sup>hep</sup> mutant mice.** **A.** c-Myc and Flag immunoblot in liver extracts of c-Jun~Fra-2<sup>hep</sup> mice treated 2 months after transgene induction with JQ1 or vehicle (VEH) during 4 weeks. Vinculin is used to control loading. **B-E.** c-Jun~Fra-2<sup>hep</sup> mutants with 9 months of transgene

## Discussion

While GEMMs are essential for advancing the cellular and molecular understanding of liver cancer (17), the combinatorial character of AP-1 homo- and hetero-dimers complicates the identification of dimer-specific functions, when using conventional monomer-based gain- or loss-of-function GEMMs. Using a single-chain, forced dimer strategy approach, the present study dissects for the first time the contribution of a specific c-Jun/Fra-2 AP-1 dimer to HCC pathogenesis *in vivo*. Hepatic expression of c-Jun~Fra-2 leads to hepatocyte proliferation, decreased hepatic fat content, moderate liver inflammation and limited fibrosis, with the subsequent development of liver tumors that have HCC characteristics. We identify a crucial pathogenic interaction between c-Jun/Fra-2 and c-Myc (Figure 6H) as an important initiating event and identify the consequences of switching off the c-Jun~Fra-2 oncogenic driver or therapeutically targeting c-Myc activation in established liver tumors.

Mice expressing Fra-1, Fra-2 or c-Jun~Fra-2 in the liver express lower levels of Ppar $\gamma$  and are protected from steatohepatitis (22, 24). Repression of Ppar $\gamma$  is maintained during liver carcinogenesis in c-Jun~Fra-2<sup>hep</sup> mice, while a c-Jun~Fra-1 dimer has apparently no effect. As Ppar $\gamma$  expression across Fra-1/2<sup>hep</sup> and c-Jun~Fra-1/2<sup>hep</sup> mice is not correlated with the occurrence of liver tumors, decreased hepatic Ppar $\gamma$  is likely not causally involved in the early c-Jun~Fra-2-driven oncogenic events. However, it might potentiate transformation, as Ppar $\gamma$ <sup>+/-</sup> mice are more susceptible to DEN-induced HCC (52). Strikingly, signs of mild inflammation, fibrosis and even ER stress, are observed in c-Jun~Fra-2<sup>hep</sup> livers despite a dyslipidemic, low hepatic fat context. Future experiments will clarify if any or all of these events are essential for tumorigenesis and how they occur independently of steatosis. The c-Jun~Fra-2<sup>hep</sup> GEMM constitutes a convenient model to dissect the interactions between pre-neoplastic or fully transformed hepatocytes and their non-parenchymal environment.

c-Myc and Myc pathway activation is a major oncogenic event in many tumor types including HCC (53, 54). A modest but consistent increase in c-Myc mRNA and protein expression was measured in livers of c-Jun~Fra-2<sup>hep</sup> mice already before tumors were observed. Importantly, and consistent with a crucial role for increased c-Myc in c-Jun~Fra-2-driven hepatocyte transformation, tumors that escaped switching off c-Jun~Fra-2 maintained c-Myc expression, while it was decreased to control levels in the adjacent non-tumoral areas. In addition, the tumor-static effect of JQ-1, which decreased Myc expression and activity in c-Jun~Fra-2 tumors, is in line with the idea that these tumors are addicted to increased c-Myc expression that is initiated by the c-Jun/Fra-2 AP-1 dimer.

Several signalling pathways, such as IL6/JAK/Stat3 and PI3K/AKT/GSK3 $\beta$  (42, 43), both elevated in c-Jun~Fra-2<sup>hep</sup> livers and tumors, can increase c-Myc expression. These pathways might also contribute to maintain c-Myc expression in tumors escaping switching off c-Jun~Fra-2, together or along with increased Fos expression that is observed in some escaping tumors. Using Jun~Fra-2<sup>hep</sup> mice, mouse and human liver cell lines and publicly available human cell lines and human liver cancer datasets, we demonstrate that c-Jun/Fra-2 activates *c-myc* transcription by binding a conserved 3' enhancer in the *c-myc* gene. Importantly, hepatocyte-specific expression of the closely related c-Jun~Fra-1 dimer, or freely dimerizing Fra-1 or Fra-2 monomers, had no impact on *c-myc* expression and did not lead to spontaneous tumors. Conversely, pre-neoplastic livers expressing Fos (19) had elevated *c-myc* mRNA, while increased *fos* mRNA was observed in three out of five tumor escapers that maintained c-Myc expression. These data indicate that only specific AP-1 complexes, such as c-Jun/Fra-2 and Fos-containing dimers can activate *c-myc* transcription in hepatocytes. Ongoing work using a similar forced dimer strategy will certainly shed light on the identity of the Fos-containing dimers modulating *c-myc* in hepatocytes. A likely consequence of this functional dimer redundancy, supported by loss-of-function experiments, is that no Jun or Fos protein is essential for *c-myc* expression. In HepG2 cells, where ChIP experiments indicate that c-Jun and Fra-2 form a functional dimer on the *MYC* 3' enhancer, knock-down of either JUN or JUNB moderately decreased *MYC* mRNA, while a significant reduction in *c-myc* mRNA and protein was observed during HBV-driven carcinogenesis in mice lacking hepatic c-Jun. However, c-Myc protein expression was unaltered in DEN-induced c-Jun <sup>$\Delta$</sup>  liver tumors, while hepatic c-Myc decreased upon genetic inactivation of the AP-1-upstream kinase JNK1

(14). Bulk RNAseq analyses of Fos-expressing and Fos-deficient livers (19) indicated that hepatic *c-myc* expression was increased in c-Fos<sup>hep</sup>, but unchanged in DEN-treated c-Fos<sup>Δλi</sup> mice. c-Myc transcription is also not affected by the single inactivation of Fra-2 in hepatocytes and Fra-2<sup>Δλi</sup> mice, subjected here for the first time to an HCC paradigm, display unaltered DEN-induced tumorigenesis. While the consequences of inactivating other AP-1 monomers, such as JunB, JunD and Fra-1 on hepatic *c-myc* expression and tumorigenesis remain to be formally tested, these experiments indicate that the requirement for AP-1-forming proteins to modulate *c-myc* expression during liver carcinogenesis is dimer- but also context- specific. Targeting one or multiple AP-1 dimers might not be a straightforward therapeutic option, although our *in silico* analysis of the TCGA-LIHC dataset, as well as preliminary immune-histochemical analyses of a set of HCC tumors, indicates that patient stratification according to JUN/FRA2 and MYC expression might help identifying patients likely to respond to such AP-1 and/or Myc-targeted therapies.

Despite being heterogeneous in size, molecular profiles and growth kinetics, liver tumors arising in Jun~Fra-2<sup>hep</sup> mice regressed upon switching off c-Jun~Fra-2 expression. However, a fraction of tumors relapsed and new tumors arose within few weeks, possibly in a c-Myc-dependent manner as indicated by the analyses of tumors collected 6 months later. The cellular and molecular events occurring immediately after turning OFF c-Jun~Fra-2, the involvement of Fos-containing dimers, and their connection to the various pro-tumorigenic functions of c-Myc certainly warrant further evaluation. Unbiased, possibly single-cell, RNA and proteome profiling of a large number of tumors in different ON and OFF settings and subsequent comparison with the OMIC data generated using c-Myc-switchable liver mice (55, 56) will help narrowing down the essential molecular and cellular players.

Several therapeutic strategies targeting Myc, mostly indirectly, have been evaluated (57, 58). The early tool compound JQ-1 (48) and other BET-family inhibitors (BETi) have preclinical benefits in several cancers, often through Myc/Myc target suppression (59). While a Myc-independent anti-tumorigenic decrease in Fra-1 transcription has been reported after BETi (60), JQ-1 does not impact c-Jun~Fra-2 mRNA or protein expression and its positive effects in c-Jun~Fra-2<sup>hep</sup> tumors appears to be Myc-dependent. This is also in line with the idea that Myc-dependent tumorigenesis is reversible even when Myc is not the initiating oncogenic lesion, as shown in lung adenocarcinoma induced by oncogenic Ras (61), an upstream activator of AP-1.

Despite a wealth of studies, there is no effective therapy for HCC due to limited mechanistic knowledge of this heterogeneous disease and the lack of biomarkers to select clinical trial patients most likely to benefit from a specific therapy. HCC prevention by limiting viral hepatitis, currently accounting for 75% of liver cancer deaths, remains the key strategy, while Sorafenib is still a standard of care for HCC in low income countries, despite limited efficacy. The increased relevance of non-viral risk factors is a major concern aggravated by the poor prognosis of HCC patients, even in high income countries with the widest portfolio of therapeutic options and where immunotherapies have become first-line treatment for advanced HCC. While BETi have shown mixed results as single agents (49, 59), immunotherapies are costly and have yet to fulfil their promises (2, 3). Combination therapies involving BET inhibitors, for example flight tested in this preclinical model, may enhance treatment effectiveness for selected patients with high AP-1/Myc expression and might help achieve widespread access to affordable and more efficient HCC treatment.

## Materials and methods

Detailed methods are provided in SI Appendix. Briefly, adult male Jun~Fra-2<sup>hep</sup> mice were sacrificed at different time point of transgene induction (typically 2 months and 9 months) and the livers harvested for histological, molecular and biochemical analyses. Blood collected by submandibular vein or cardiac puncture was used for longitudinal monitoring. Murine AML12 and human HepG2 liver-derived cell lines were used for *in vitro* experiments.

## Data, Materials, and Software Availability

All data relevant to the study are included in the article and/or SI Appendix. RNAseq datasets are deposited as series: GSE261005 in the Gene expression omnibus (GEO) archive <https://www.ncbi.nlm.nih.gov/geo/>.

Non-commercially available materials and reagents are available upon reasonable request.

### Acknowledgments and funding sources

We thank Guillermo Medrano for help with mouse procedures and Vanessa Bermeo for assisting with tissue sections and staining. Birgit Hockenjos for analysing Jun<sup>Δλλ</sup>, HBV<sup>Tg</sup> liver samples, Stefanie Stolzlechner for IHC troubleshooting and Sophia Derdak from the Core Facilities of the MUV, a member of the Vienna Life-Science Instruments initiative, for analysis of bulk RNA-seq data. We are grateful to the CNIO Molecular Imaging, Mouse Genome Editing, Histopathology and Genomics Core Units for efficient service. We are very grateful to Drs. Douglas Hanahan, Kazuhiko Matsuoka, Robert Eferl, Nabil Djouder, Esteban Gurzov, Emilio Casanova and to the members of the Wagner laboratory for comments and discussions. The Wagner laboratory is supported by the ERC (AdG 2016-741888-CSI-Fun), a H2020 – MSCA grant (ITN 2019-859860-CANCERPREV) and the MUW.

### References

1. H. Sung *et al.* , Global Cancer Statistics 2020: GLOBOCAN Estimates of Incidence and Mortality Worldwide for 36 Cancers in 185 Countries. *CA Cancer J Clin* **71** , 209-249 (2021).
2. A. Alqahtani *et al.* , Hepatocellular Carcinoma: Molecular Mechanisms and Targeted Therapies. *Medicina (Kaunas)* **55**(2019).
3. J. Hou, H. Zhang, B. Sun, M. Karin, The immunobiology of hepatocellular carcinoma in humans and mice: Basic concepts and therapeutic implications. *J Hepatol* **72** , 167-182 (2020).
4. C. Campani, J. Zucman-Rossi, J. C. Nault, Genetics of Hepatocellular Carcinoma: From Tumor to Circulating DNA. *Cancers (Basel)***15** (2023).
5. G. He, M. Karin, NF-kappaB and STAT3 - key players in liver inflammation and cancer. *Cell Res* **21** , 159-168 (2011).
6. E. F. Wagner, A. R. Nebreda, Signal integration by JNK and p38 MAPK pathways in cancer development. *Nat Rev Cancer* **9** , 537-549 (2009).
7. R. Eferl, E. F. Wagner, AP-1: a double-edged sword in tumorigenesis. *Nat Rev Cancer* **3** , 859-868 (2003).
8. G. L. Rampioni Vinciguerra *et al.* , Role of Fra-2 in cancer. *Cell Death Differ* 10.1038/s41418-023-01248-4 (2023).
9. E. Stepniak *et al.* , c-Jun/AP-1 controls liver regeneration by repressing p53/p21 and p38 MAPK activity. *Genes Dev* **20** , 2306-2314 (2006).
10. I. Schulien *et al.* , The transcription factor c-Jun/AP-1 promotes liver fibrosis during non-alcoholic steatohepatitis by regulating Osteopontin expression. *Cell Death Differ* **26** , 1688-1699 (2019).
11. P. Hasselblatt, M. Rath, V. Komnenovic, K. Zatloukal, E. F. Wagner, Hepatocyte survival in acute hepatitis is due to c-Jun/AP-1-dependent expression of inducible nitric oxide synthase. *Proc Natl Acad Sci U S A* **104** , 17105-17110 (2007).
12. M. Fuest *et al.* , The transcription factor c-Jun protects against sustained hepatic endoplasmic reticulum stress thereby promoting hepatocyte survival. *Hepatology* **55** , 408-418 (2012).
13. R. Eferl *et al.* , Liver tumor development. c-Jun antagonizes the proapoptotic activity of p53. *Cell* **112** , 181-192 (2003).
14. L. Hui, K. Zatloukal, H. Scheuch, E. Stepniak, E. F. Wagner, Proliferation of human HCC cells and chemically induced mouse liver cancers requires JNK1-dependent p21 downregulation. *J Clin Invest***118** , 3943-3953 (2008).

15. K. Machida *et al.* , c-Jun mediates hepatitis C virus hepatocarcinogenesis through signal transducer and activator of transcription 3 and nitric oxide-dependent impairment of oxidative DNA repair. *Hepatology* **52** , 480-492 (2010).
16. L. Min *et al.* , Liver cancer initiation is controlled by AP-1 through SIRT6-dependent inhibition of survivin. *Nat Cell Biol***14** , 1203-1211 (2012).
17. L. Bakiri, E. F. Wagner, Mouse models for liver cancer. *Mol Oncol* **7** , 206-223 (2013).
18. C. Trierweiler *et al.* , The transcription factor c-JUN/AP-1 promotes HBV-related liver tumorigenesis in mice. *Cell Death Differ* **23** , 576-582 (2016).
19. L. Bakiri *et al.* , Liver carcinogenesis by FOS-dependent inflammation and cholesterol dysregulation. *J Exp Med***214** , 1387-1409 (2017).
20. M. K. Thomsen *et al.* , JUNB/AP-1 controls IFN-gamma during inflammatory liver disease. *J Clin Invest* **123** , 5258-5268 (2013).
21. D. E. Smart *et al.* , JunD is a profibrogenic transcription factor regulated by Jun N-terminal kinase-independent phosphorylation. *Hepatology* **44** , 1432-1440 (2006).
22. S. C. Hasenfuss *et al.* , Regulation of steatohepatitis and PPARgamma signaling by distinct AP-1 dimers. *Cell Metab***19** , 84-95 (2014).
23. S. C. Hasenfuss, L. Bakiri, M. K. Thomsen, R. Hamacher, E. F. Wagner, Activator Protein 1 transcription factor Fos-related antigen 1 (Fra-1) is dispensable for murine liver fibrosis, but modulates xenobiotic metabolism. *Hepatology* **59** , 261-273 (2014).
24. L. Bakiri, S. C. Hasenfuss, E. F. Wagner, A FATal AP-1 dimer switch in hepatosteatosis. *Cell Cycle* **13** , 1218-1219 (2014).
25. L. Bakiri, K. Matsuo, M. Wisniewska, E. F. Wagner, M. Yaniv, Promoter specificity and biological activity of tethered AP-1 dimers. *Mol Cell Biol* **22** , 4952-4964 (2002).
26. A. Kobeissy *et al.* , Protein Induced by Vitamin K Absence or Antagonist-II Versus Alpha-Fetoprotein in the Diagnosis of Hepatocellular Carcinoma: A Systematic Review With Meta-Analysis. *J Clin Med Res* **15** , 343-359 (2023).
27. X. Zhou *et al.* , MCM2 promotes the stemness and sorafenib resistance of hepatocellular carcinoma cells via hippo signaling. *Cell Death Discov* **8** , 418 (2022).
28. M. Wang *et al.* , SOX9 enhances sorafenib resistance through upregulating ABCG2 expression in hepatocellular carcinoma. *Biomed Pharmacother* **129** , 110315 (2020).
29. M. B. Ruzinova *et al.* , SOX9 Expression Is Superior to Other Stem Cell Markers K19 and EpCAM in Predicting Prognosis in Hepatocellular Carcinoma. *Am J Surg Pathol* **47** , 1-11 (2023).
30. A. Subramanian *et al.* , Gene set enrichment analysis: a knowledge-based approach for interpreting genome-wide expression profiles. *Proc Natl Acad Sci U S A* **102** , 15545-15550 (2005).
31. A. M. Newman *et al.* , Determining cell type abundance and expression from bulk tissues with digital cytometry. *Nat Biotechnol* **37** , 773-782 (2019).
32. R. Carlessi *et al.* , Single-nucleus RNA sequencing of pre-malignant liver reveals disease-associated hepatocyte state with HCC prognostic potential. *Cell Genom* **3** , 100301 (2023).
33. Y. Hoshida *et al.* , Integrative transcriptome analysis reveals common molecular subclasses of human hepatocellular carcinoma. *Cancer Res* **69** , 7385-7392 (2009).
34. S. Boyault *et al.* , Transcriptome classification of HCC is related to gene alterations and to new therapeutic targets. *Hepatology* **45** , 42-52 (2007).

35. H. G. Woo *et al.* , Identification of a cholangiocarcinoma-like gene expression trait in hepatocellular carcinoma. *Cancer Res***70** , 3034-3041 (2010).
36. J. S. Lee *et al.* , A novel prognostic subtype of human hepatocellular carcinoma derived from hepatic progenitor cells. *Nat Med* **12** , 410-416 (2006).
37. S. Cairo *et al.* , Hepatic stem-like phenotype and interplay of Wnt/beta-catenin and Myc signaling in aggressive childhood liver cancer. *Cancer Cell* **14** , 471-484 (2008).
38. J. S. Lee *et al.* , Application of comparative functional genomics to identify best-fit mouse models to study human cancer. *Nat Genet* **36** , 1306-1311 (2004).
39. N. Aizarani *et al.* , A human liver cell atlas reveals heterogeneity and epithelial progenitors. *Nature* **572** , 199-204 (2019).
40. L. Zhou *et al.* , Integrated Analysis Highlights the Immunosuppressive Role of TREM2(+) Macrophages in Hepatocellular Carcinoma. *Front Immunol* **13** , 848367 (2022).
41. Y. Liao, J. Wang, E. J. Jaehnig, Z. Shi, B. Zhang, WebGestalt 2019: gene set analysis toolkit with revamped UIs and APIs. *Nucleic Acids Res* **47** , W199-W205 (2019).
42. N. Kiuchi *et al.* , STAT3 is required for the gp130-mediated full activation of the c-myc gene. *J Exp Med* **189** , 63-73 (1999).
43. E. J. Sun, M. Wankell, P. Palamuthusingam, C. McFarlane, L. Hebbard, Targeting the PI3K/Akt/mTOR Pathway in Hepatocellular Carcinoma. *Biomedicines* **9** (2021).
44. B. N. Song, I. S. Chu, A gene expression signature of FOXM1 predicts the prognosis of hepatocellular carcinoma. *Exp Mol Med***50** , e418 (2018).
45. G. S. Yochum, R. Cleland, R. H. Goodman, A genome-wide screen for beta-catenin binding sites identifies a downstream enhancer element that controls c-Myc gene expression. *Mol Cell Biol* **28** , 7368-7379 (2008).
46. E. C. Partridge *et al.* , Occupancy maps of 208 chromatin-associated proteins in one human cell type. *Nature***583** , 720-728 (2020).
47. C. G. A. R. Network., Comprehensive and Integrative Genomic Characterization of Hepatocellular Carcinoma. *Cell* **169** , 1327-1341 e1323 (2017).
48. P. Filippakopoulos *et al.* , Selective inhibition of BET bromodomains. *Nature* **468** , 1067-1073 (2010).
49. M. P. Schwalm, S. Knapp, BET bromodomain inhibitors. *Curr Opin Chem Biol* **68** , 102148 (2022).
50. S. Hagiwara *et al.* , Activation of JNK and high expression level of CD133 predict a poor response to sorafenib in hepatocellular carcinoma. *Br J Cancer* **106** , 1997-2003 (2012).
51. W. Chen *et al.* , Activation of c-Jun predicts a poor response to sorafenib in hepatocellular carcinoma: Preliminary Clinical Evidence. *Sci Rep* **6** , 22976 (2016).
52. J. Yu *et al.* , Inhibitory role of peroxisome proliferator-activated receptor gamma in hepatocarcinogenesis in mice and in vitro. *Hepatology* **51** , 2008-2019 (2010).
53. F. X. Schaub *et al.* , Pan-cancer Alterations of the MYC Oncogene and Its Proximal Network across the Cancer Genome Atlas. *Cell Syst* **6** , 282-300 e282 (2018).
54. M. Gabay, Y. Li, D. W. Felsher, MYC activation is a hallmark of cancer initiation and maintenance. *Cold Spring Harb Perspect Med***4** (2014).
55. R. Dhanasekaran *et al.* , MYC Overexpression Drives Immune Evasion in Hepatocellular Carcinoma That Is Reversible through Restoration of Proinflammatory Macrophages. *Cancer Res***83** , 626-640 (2023).

56. T. R. Kress *et al.* , Identification of MYC-Dependent Transcriptional Programs in Oncogene-Addicted Liver Tumors. *Cancer Res* **76** , 3463-3472 (2016).
57. B. L. Allen-Petersen, R. C. Sears, Mission Possible: Advances in MYC Therapeutic Targeting in Cancer. *BioDrugs* **33** , 539-553 (2019).
58. J. R. Whitfield, L. Soucek, The long journey to bring a Myc inhibitor to the clinic. *J Cell Biol* **220** (2021).
59. A. G. Cochran, A. R. Conery, R. J. Sims, 3rd, Bromodomains: a new target class for drug development. *Nat Rev Drug Discov* **18** , 609-628 (2019).
60. E. K. Baker *et al.* , BET inhibitors induce apoptosis through a MYC independent mechanism and synergise with CDK inhibitors to kill osteosarcoma cells. *Sci Rep* **5** , 10120 (2015).
61. L. Soucek *et al.* , Modelling Myc inhibition as a cancer therapy. *Nature* **455** , 679-683 (2008).

## SI APPENDIX :

### **This PDF file includes:**

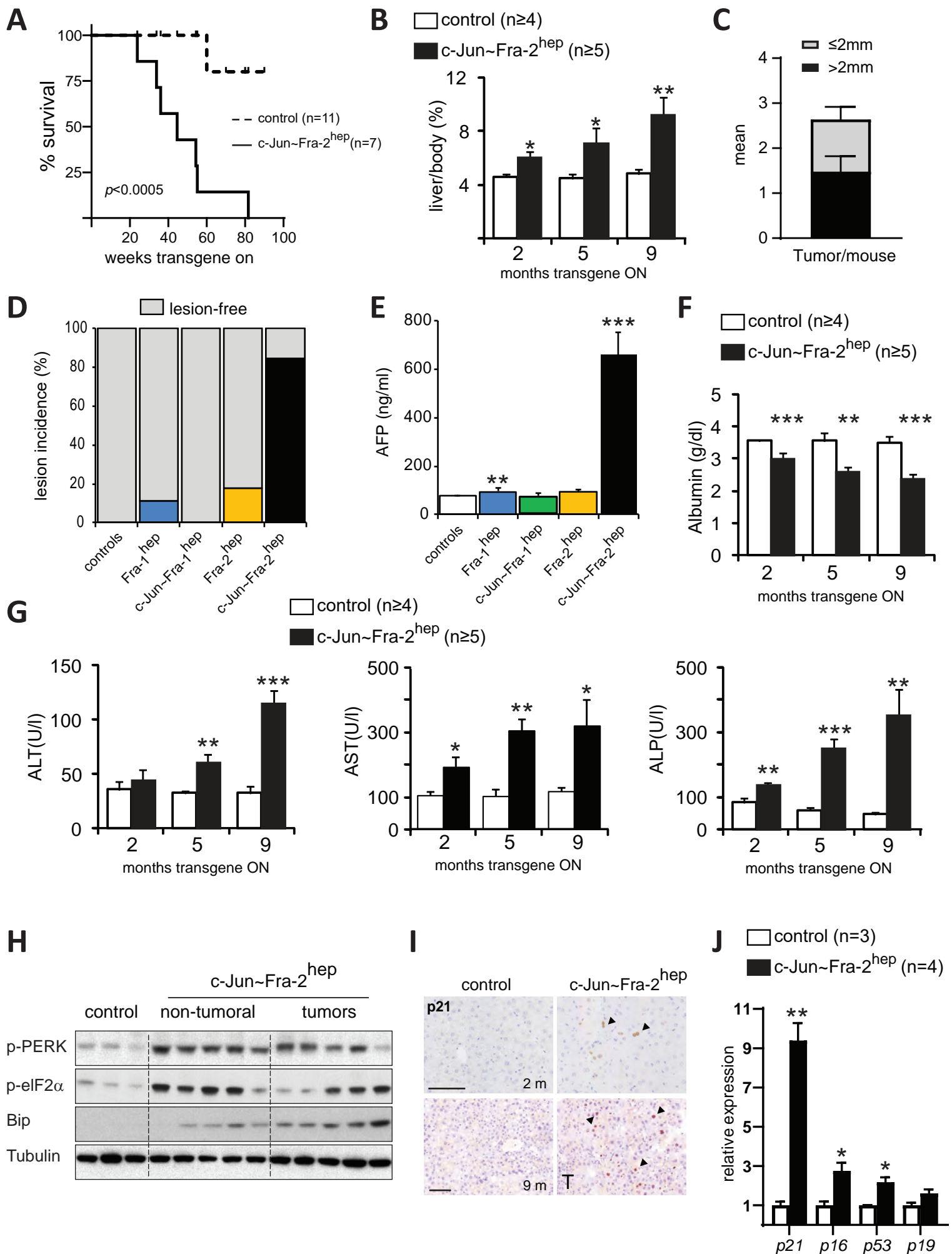
Supplementary Figure legends

Supplementary Materials and Methods

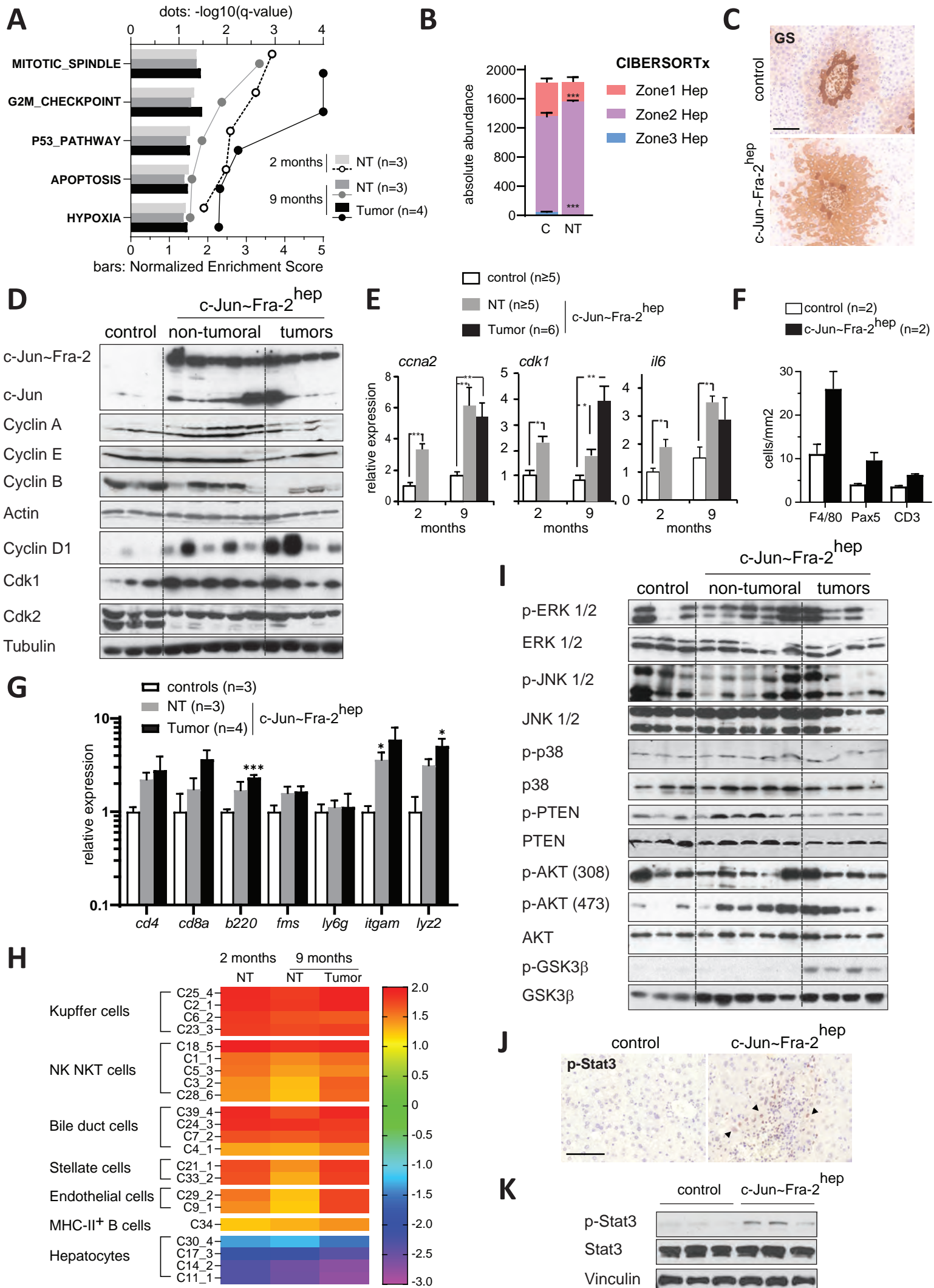
Supplementary References

Supplementary Figures 1 to 7

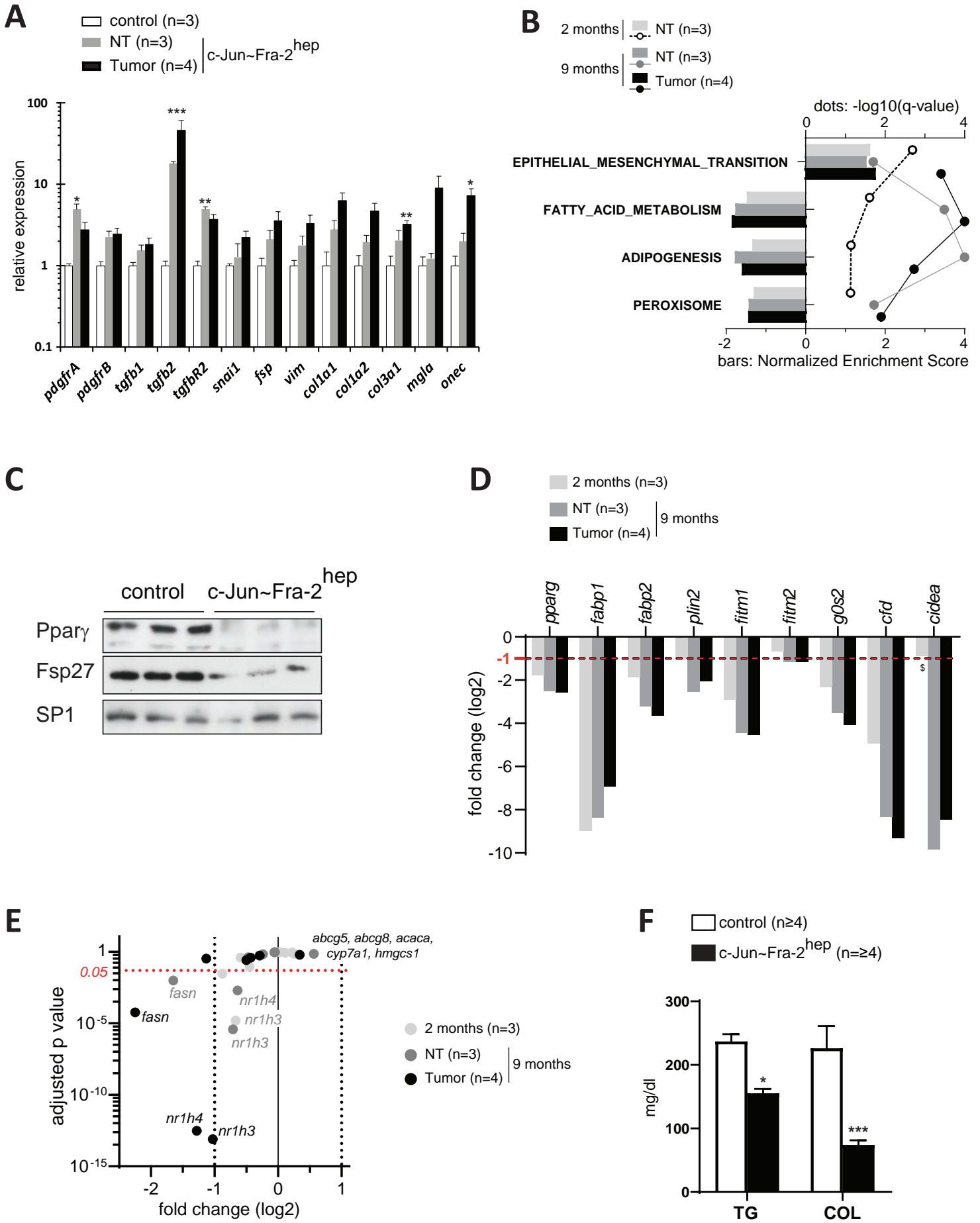
Supplementary Tables 1 to 3



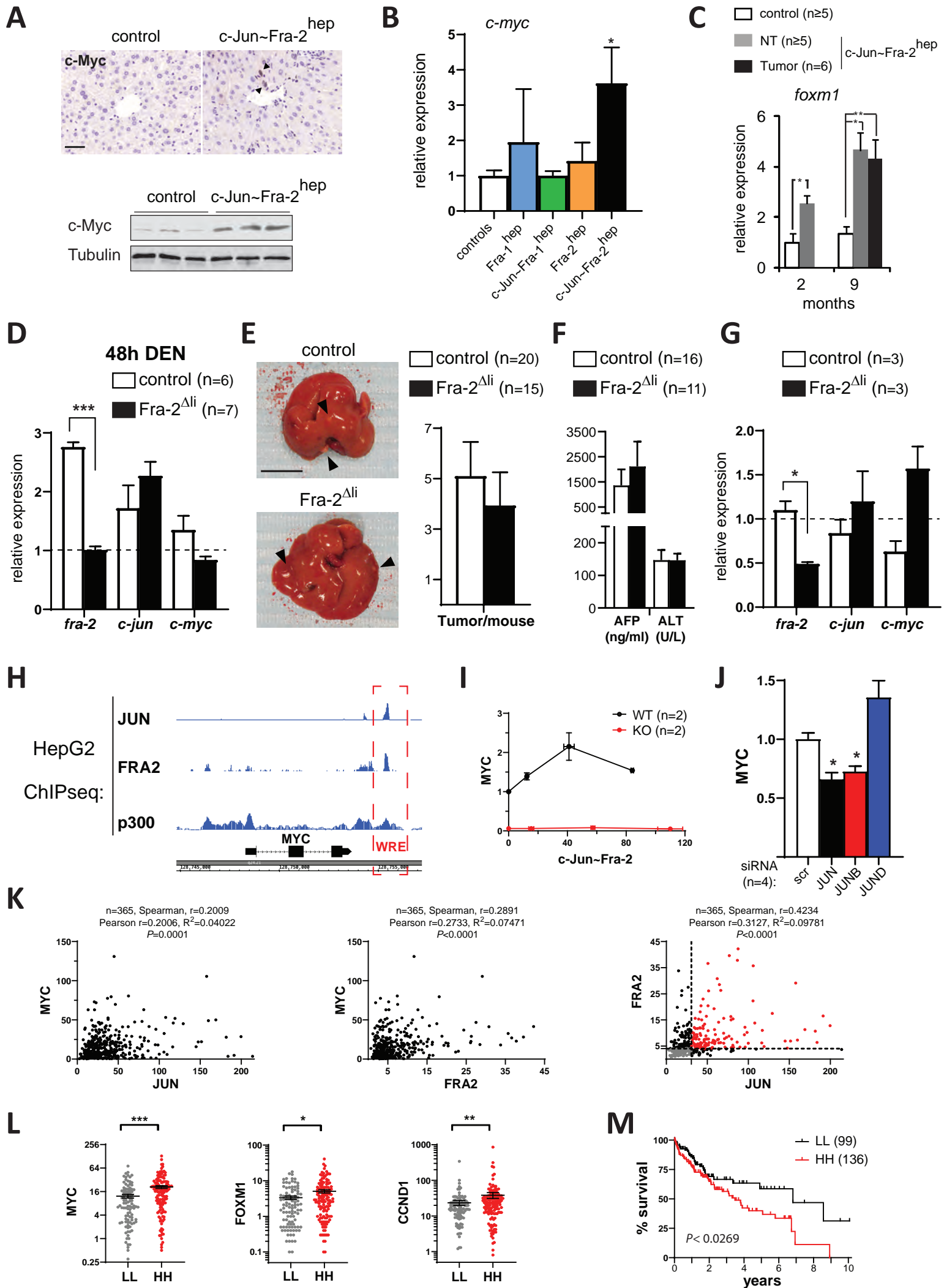
Sup Figure 1. Bakiri et al.



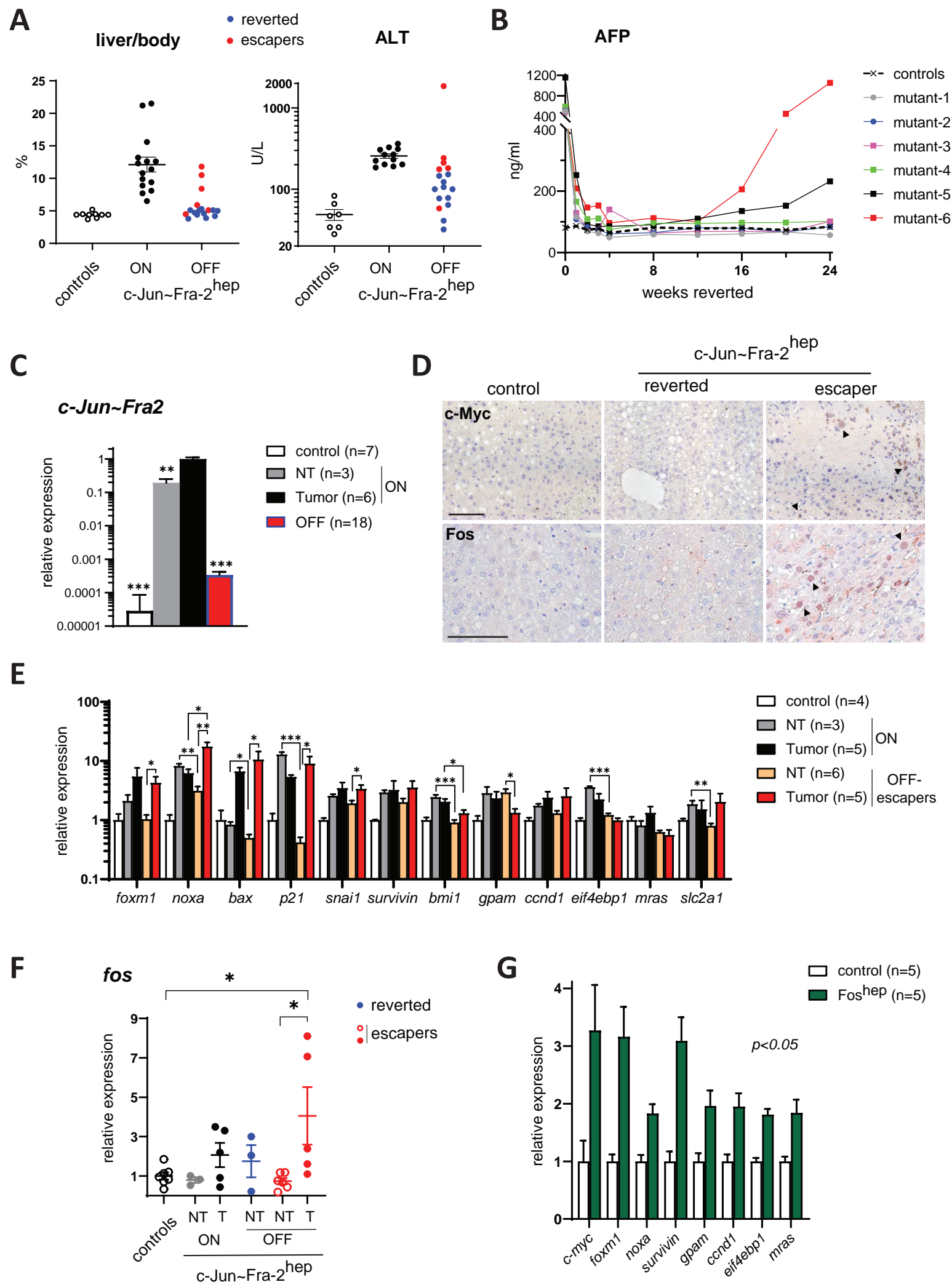
Sup Figure 2. Bakiri et al.



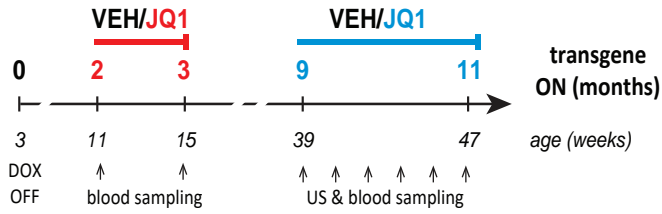
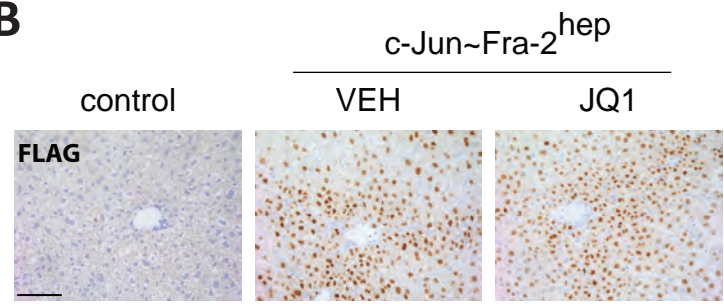
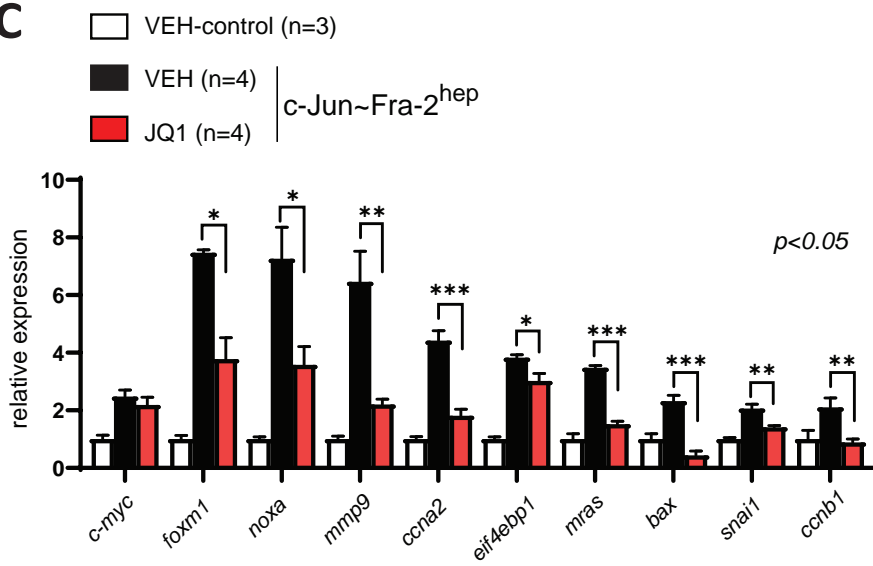
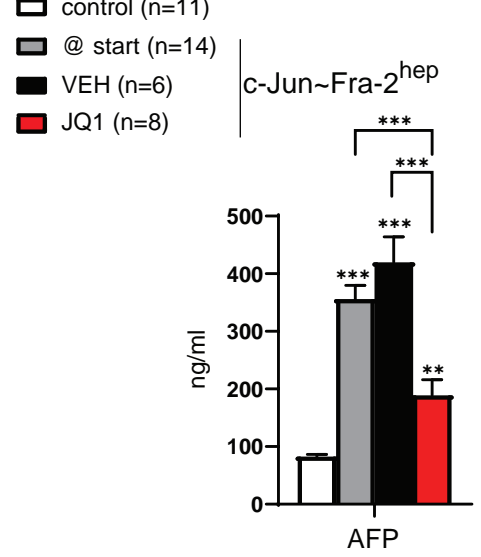
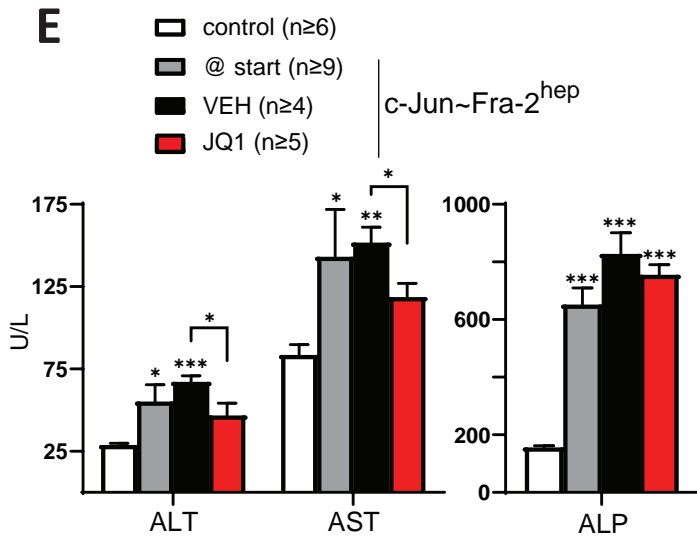
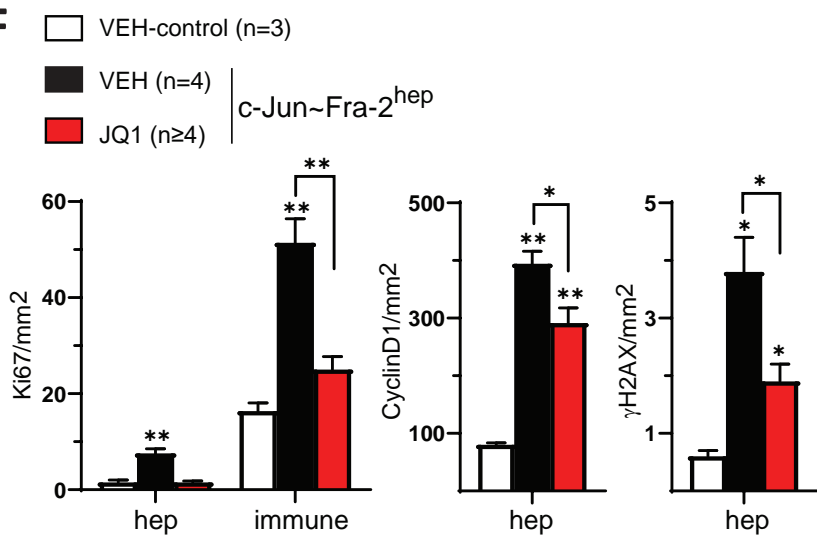
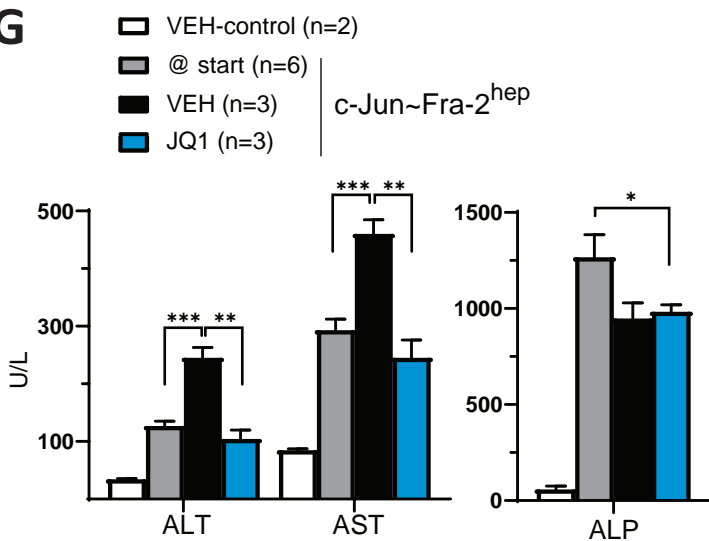
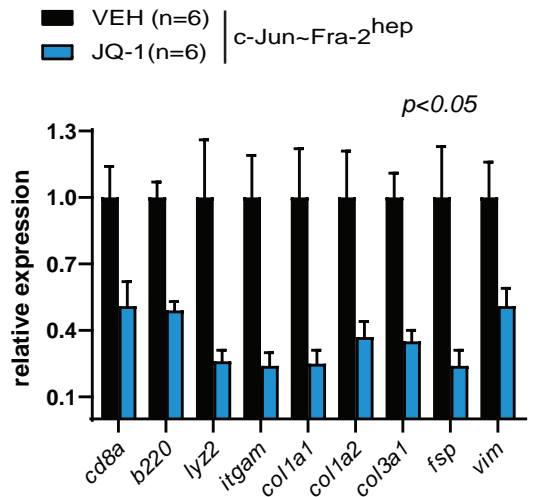
Sup Figure 3. Bakiri et al.

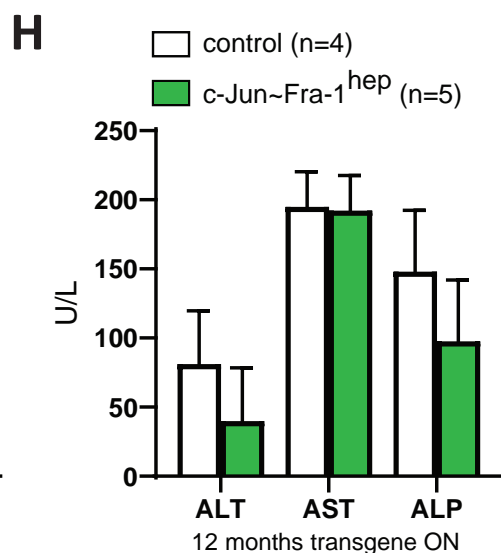
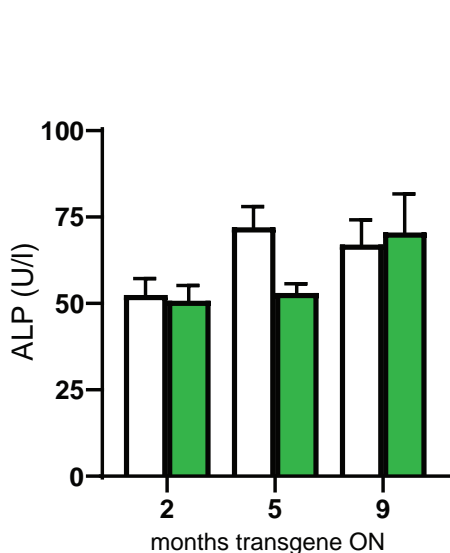
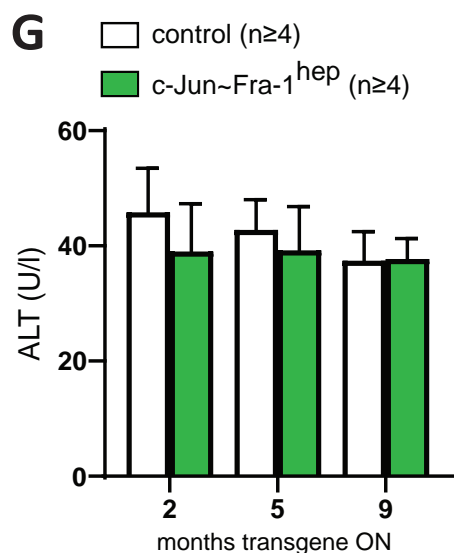
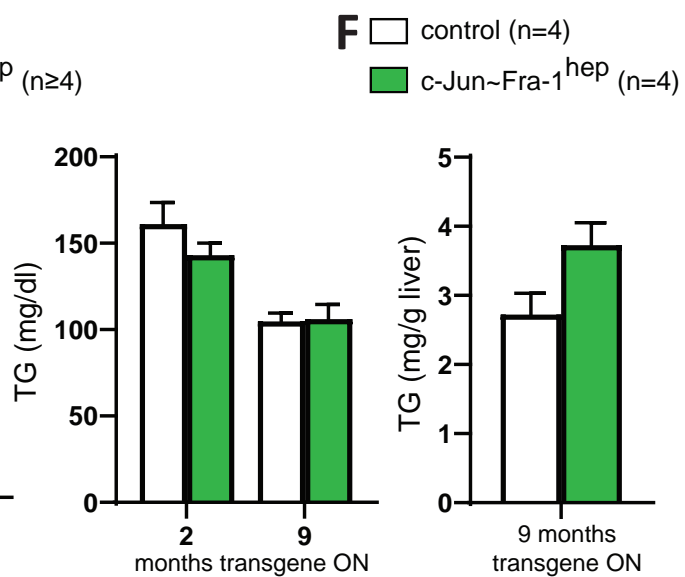
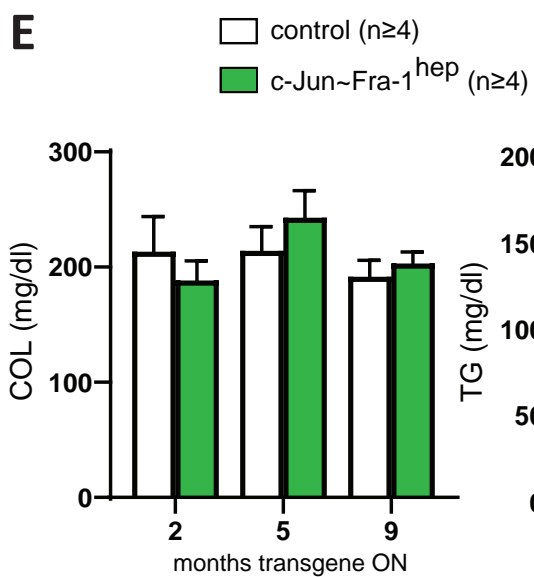
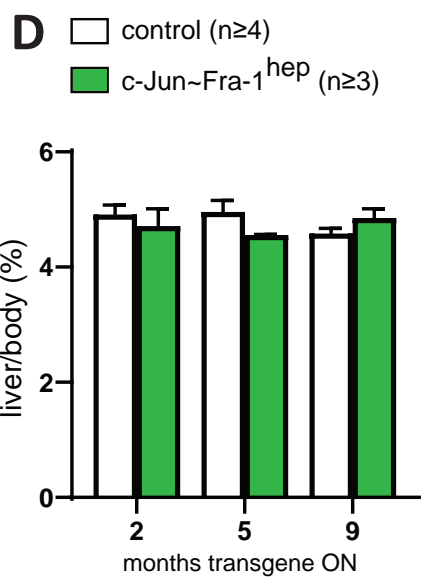
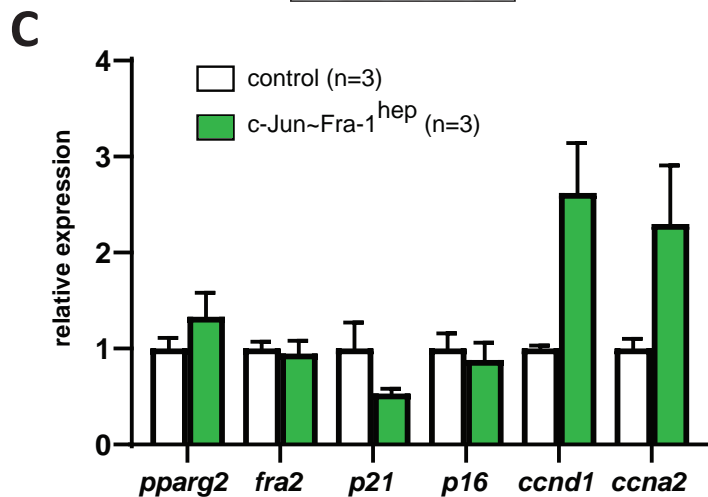
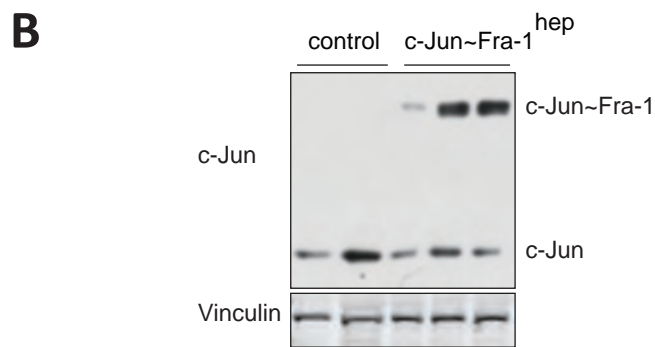
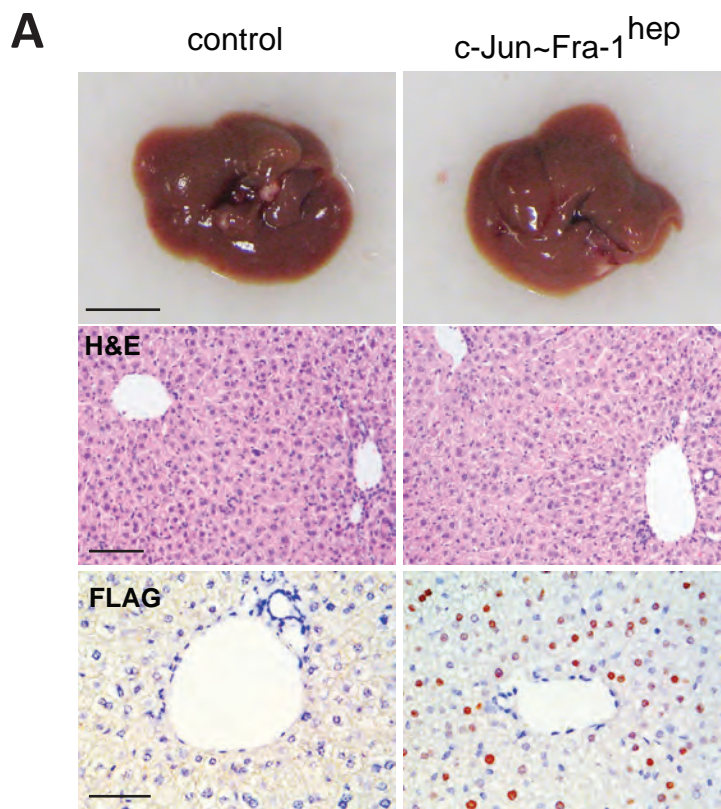


Sup Figure 4. Bakiri et al.



Sup Figure 5. Bakiri et al.

**A****B****C****D****E****F****G****H**



**A**

	Tumors		mean T.vol (mm3)		T.burden (mm3)		AFP (ng/ml)		ALT (U/L)		ALP (U/L)	
	start	end	start	end	start	end	start	end	start	end	start	end
mutant-1	1	-	0.4	-	0.4	-	503	57	173	31	1,168	144
mutant-2	2	-	5.5	-	10.9	-	514	84	149	77	744	188
mutant-3	2	1+1*	42.3	12.8	84.6	25.5	489	101	133	36	1,152	200
mutant-4	3	1+1*	62.0	4.4	185.9	8.9	589	102	138	84	1,008	204
mutant-5	1	2+1*	95.3	35.2	95.3	211.4	1,158	232	99	232	1,080	272
mutant-6	2	2+1*	591.5	272.6	1,183.1	1,090.3	580	1,054	208	742	948	111
control-1	<i>not applicable</i>						85	95	27	57	183	190
control-2	<i>not applicable</i>						76	72	36	22	138	150

**B**

	group	Tumors		T.burden (mm3)		liver/body (%, end)	AFP (ng/ml)		ALT (U/L)		AST (U/L)		ALP (U/L)	
		start	end	start	end		start	end	start	end	start	end		
mutant-1	VEH	5	5+3*	27.1	1,320.9	12.6	583	727	91	202	326	404	1,584	780
mutant-2	VEH	1	1+3*	6.7	251.3	13.2	663	1,063	150	268	330	468	1,272	940
mutant-3	VEH	1	1+4*	3.4	127.9	9.9	540	675	138	266	348	508	1,056	1,124
mutant-4	JQ1	3	3	45.6	351.2	9.6	634	160	108	136	282	309	1,436	1,008
mutant-5	JQ1	2	2	8.8	28.1	8.3	451	136	142	106	212	248	749	1,044
mutant-6	JQ1	2	2	4.6	33.1	7.9	485	144	131	72	260	178	1,504	896
control-1	none	<i>not applicable</i>				4.4	58	74	36	28	86	88	137	190
control-2		<i>not applicable</i>				4.4	52	53	34	34	76	108	139	170

**Table S2.** Oligonucleotides used in the study**Murine RT-qPCR primers**

<b>Product</b>	<b>Forward primer (5'-3')</b>	<b>Reverse primer (5'-3')</b>
<i>afp</i>	GTATGGACTCTCAGGCTGCT	GAAGGGGTTCTCCTTGACA
<i>asma</i>	CAATGGCTCTGGGCTCTGTA	TCATCCCCACATAGCTGTC
<i>b220</i>	GGGTTGTTCTGTGCCTTGTT	GGATAGATGCTGGCGATGAT
<i>bax</i>	TCTGGATCCAAGACCAGG	GGACTCCAGCCACAAAGAT
<i>bex1</i>	CCTAACGGAGGCACCTGTT	CGCCTTGATCTTTGGACTCC
<i>bmi1</i>	GCTTGGCTCGCATTCAATT	GGACACACATTAAGTGGGGA
<i>ccna2</i>	AGAGGCAGCCAGACATCACT	AAGCTAGCAGCATAGCAGCC
<i>ccnb1</i>	CATAGGATACCTACCGTGTT	GTTAGCCTAAACTCAGAAGC
<i>ccnd1</i>	TGCTGCAAATGGAAGTCTT	GGTCTGCTTGTCTCATCCG
<i>cd133</i>	TGCAGCAATCACTGAATACG	AACAGAGTCCAAAGAGGCAA
<i>cd163</i>	CTCTGCTGTCACTAACGCTC	GGACACTTCATTATGCTCC
<i>cd44</i>	GCACTGTGACTCATGGATCC	TTCTGGAATCTGAGGTCTCC
<i>cd68</i>	TGATCTTGCTAGGACCGCTT	GGAGCTGGTGTGAACTGTGA
<i>cd8a</i>	TCAGTTCTGTCGTGCCAGTC	ATCACAGGCGAAGTCCAATC
<i>cdk1</i>	GTCCCTGCAGGACTACAAGA	TTGAGAGCAAATCCAAGCCG
<i>c-fos</i>	CCAGTCAAGAGCATCAGCAA	TAAGTAGTGACCCCGGAGT
<i>c-jun</i>	AGTCTCAGGAGCGGATCAAG	TGAGTTGGCACCCTGTTA
<i>c-myc</i>	TCACCAGCACAACACTACGCCG	TGCTTCAGGACCCTGCCACT
<i>col1a1</i>	CATGTTCAAGCTTTGTGGACCT	TAGGCCATTGTGTATGCAGC
<i>col1a2</i>	GCTGGAATCCGAGGTCCTAA	GCCAACATTTCCAGGAGACC
<i>col3a1</i>	AAAGAGGATCTGAGGGCTCG	GCCACCAGACTTTTCACCTC
<i>dlk1</i>	TGGAGTCTGCAAGGAACCAT	TGGCAGGGAGAACCATTGAT
<i>efi4ebp1</i>	ACTAGCCCTACCAGCGAT	TACGGCTGGTCCCTTAAATG
<i>fms</i>	CATGGCCTTCCTTGCTTCTAA	TGCCGTAGGACCACACATCA
<i>foxm1</i>	ATTCACCCAAGTGCCAATCG	ATTGGGTCGTTTCTGCTGTG
<i>fra-2</i>	TGGAGTGATCAAGACCATCG	AGCTAGCTTGTTTCTCTCCC
<i>cjun-fra2</i>	CTCACCGCAGAAGCAGTA	TGTCGTCGTCGTCCTTGTAG
<i>fsp</i>	TGAGCAACTTGGACAGCAACA	TTCCGGGGTTCCTTATCTGGG
<i>gp73</i>	AGAAGCTCATTGAGACCTG	CATCTGGCTGATACACTGGT
<i>gpam</i>	GCGGGGTCAGCACAT	AGGCTCTCCTTCCATTTAG
<i>gpc3</i>	GTGACGGGATGGTGAAAGTG	TGTGAGAGGTGGTGTCTCG
<i>h19</i>	CCTCCCACGCAAGTTCAATT	ACCGGACCATGTCATGTCTT
<i>il6</i>	CAAAGCCAGAGTCCTTCAGAG	TGGTCTTGGTCCCTTAGCCAC
<i>itgam</i>	CCAAGACGATCTCAGCATCA	TAGCAGGAAAGATGGGATGG
<i>ly6d</i>	AGGATGAAGACAGCTCTGC	AGAAGTAGAAGTTGGACGGG
<i>ly6g</i>	CATTGCAAAGTCCTGTGTGC	AGGGGCAGGTAGTTGTGTTG
<i>lyz2</i>	TTAGCTCAGCACGAGAGCA	CACTGCAATTGATCCCACAG
<i>marco</i>	GAAGACTTCTTGGGCAGCAC	GTGAGCAGGATCAGGTGGAT
<i>mcm2</i>	CTTTGTAAGTGGGGCCTTTCT	GATGCGGATACGTTGGTAGT
<i>mgla</i>	CAGGAGAAATGCCAACACCT	GCGTTGTAGCCGTAGACCAT
<i>mmp9</i>	TCCCCAAAGACCTGAAAACC	TAGAGACTGCTTCTCTCCCA
<i>mras</i>	GAGAAGTCGCTCACCCT	CATGTTTCTGGTAGTCAGGC
<i>mrc1</i>	CACTTTCAATGCCTGGACTG	GCCACCAATCACAACACTACAC
<i>nope</i>	GGGGTAGGGAGTGAAACCAA	CCGCCCTTTTCTATGCAAA
<i>noxa</i>	GTGCACCGGACATAACTGTG	GGAGTTGAGCACACTCGT

<i>onec</i>	AGAGCTCCAAGAGGCTTCC	GAAAGAAGATCCAGGCCCTC
<i>p16</i>	CTTGGTCACTGTGAGGATTCAG	GTGAACGTTGCCATCATCA
<i>p19</i>	CCAAGATGCCTCCGGTACTA	CCCTCTTTATCGCCAGATG
<i>p21</i>	CAGAGTCTAGGGGAATTGGA	GTCGGACATCACCAGGATT
<i>p53</i>	AAGATCCGCGGGCGTAA	CATCCTTTAACTCTAAGGCCTCATT
<i>pdgfrA</i>	TGGAGCTTGAGGGAGAGAAA	AGAAAGACCTGGTGGGAGGT
<i>pdgfrB</i>	GAGTTTGCTCTTGTCCTCGAG	AGGACAGCTGTAAGGGGGTT
<i>pparg2</i>	GAAGTTGGTGGGCCAGAATG	TTGACCCAGAGCATGGTGC
<i>rpl4</i>	CTACTGCACTGGCAACAAA	TCTTGGCAACCACCTTTTTC
<i>rps29</i>	ATGGGTCACCAGCAGCTCTA	GCCTATGTCCTTCGCGTACT
<i>slc2a1</i>	GCGGGAGACGCATAGTTA	GACACCAGTGTTATAGCCGA
<i>snai1</i>	CATGTCTGGACCTGGTTCCT	AAGGGTCCTTGAGGGAGGTA
<i>sox9</i>	GTTGATCTGAAGCGAGAGGG	CATTGACGTCGAAGGTCTCA
<i>survivin</i>	TGGCAGCTGTACCTCAAGAA	TCCCAGCCTTCCAATTCCTT
<i>tgfb1</i>	GTCCTTGCCCTCTACAACCA	GTTGGACAACCTGCTCCACCT
<i>tgfb2</i>	CCCACATCTCTGCTAATGT	CGAAGGCAGCAATTATCCTG
<i>tgfbR2</i>	GGACCCTACTCTGTCTGTGG	TGGAGTAGACATCCGTCTGC
<i>vim</i>	GTGCGCCAGCAGTATGAAAG	GCATCGTTGTTCCGGTTGG

**Murine CHIP-qPCR primers**

<b>Product</b>	<b>Forward primer (5'-3')</b>	<b>Reverse primer (5'-3')</b>
myc WRE	CAGGCAAGCCCAAAGAATAG	CCCACAGCCAAATCTGAATC
myc Promoter	CTTTGACACGTCCAGCTTAC	CCTAGTTGTGGATGGGGAAA
Dusp1 promoter	TGGCAAAACCCATTGATGTC	AGAAAGGGGAAAGCGAATCT
intergenic	CAGTTCACACATATAAAGCAG	GTTGTTGTTGTTGCTTCACTG

**Human RT-qPCR primers**

<b>Product</b>	<b>Forward primer (5'-3')</b>	<b>Reverse primer (5'-3')</b>
<i>MYC</i>	CACCGAGTCGTAGTCGAGGT	GCTGCTTAGACGCTGGATTT
<i>RPL29</i>	CTTCCGGTTCTAGGCGCTT	ATTTTCGGGACTGGTTGTGTGT
<i>RPS29</i>	ATGGGTCACCAGCAGCTCTA	GCCTATGTCCTTCGCGTACT

**Table S3.** Antibodies used in the study

<b>Antigen</b>	<b>Supplier</b>	<b>Reference</b>
Actin	Sigma	A4700
AFP	R&D	AF5369
AKT	Cell Signaling	9272
Bex1/2	Santa Cruz	sc-98915
Bip	Cell Signaling	3183
CD3	Roche	790-4341
Cdk1	Pharmingen	558900
Cdk2	Sigma	C5223
c-Fos	Cell Signaling	2250
c-Jun	Cell Signaling	9165
c-Myc (IB)	Santa Cruz	sc-42
c-Myc (IHC)	Abcam	ab32072
Cyclin A	Sigma	C4710
Cyclin B	Sigma	C8831
Cyclin D1 (IB)	home made	Jiri Bartek
Cyclin D1 (IHC)	DAKO	M3635
Cyclin E	Upstate	07-687
ERK1/2	Cell Signaling	9102
F4/80	Biorad	MCA497R
Flag	Sigma	F3165
Fra-2	Sigma	MABS1261
Fsp27	Novus Biologicals	NB100-430
Gapdh	Sigma	G8795
$\gamma$ H2AX	Millipore	05-636
GP73	Santa Cruz	sc-48011
GSK3 $\beta$	Cell Signaling	9332
H2A	Cell Signaling	2578
IgG	Millipore	12-371B
JNK1/2	Cell Signaling	9252
Ki67	Dako	M7249
Mcm2	BD	610700
p19	Santa Cruz	sc-7403
p21	Abcam	ab107099
p38	Cell Signaling	9218
p53	Leica	NCL-p53-CM5p
p65	Santa Cruz	sc-372
p-AKT (308)	Cell Signaling	9275
p-AKT (473)	Cell Signaling	9271
Pax5	Santa Cruz	sc-1974
PERK	Cell Signaling	3192
p-ERK1/2	Cell Signaling	9106
p-GSK3 $\beta$	Cell Signaling	9336
p-JNK1/2	Cell Signaling	9251
p-p38	Cell Signaling	9211
p-p65	Cell Signaling	3037
Ppary	Cell Signaling	2443

p-PERK	Cell Signaling	3179
p-PTEN	Cell Signaling	9551
p-Smad2	Cell Signaling	3101
p-Stat3	Cell Signaling	9131
PTEN	Cell Signaling	9559
Smad2	Cell signaling	3103
Sox9	Millipore	AB5535
SP1	Santa Cruz	sc-059
Stat3	Cell Signaling	9132
Tubulin	Sigma	T9026
Vinculin	Sigma	V4505

## Supplementary Figure legends

### Supplementary Figure 1: Related to Figure 1

**A.** Survival of c-Jun~Fra<sup>hep</sup> and control mice off Dox since weaning ( $p$  by Mantel-Cox Log-rank test). **B.** Liver/body weight ratio over time in c-Jun~Fra-2<sup>hep</sup> mice and controls (n=control/mutant: 8/6, 4/5, 7/7). **C.** Mean number of small ( $\leq 2$ mm) and large ( $> 2$ mm) hepatic surface nodules in c-Jun~Fra<sup>hep</sup> mice at 9 months of transgene expression (n=31). Comparison of macroscopic liver lesion incidence (**D**) and serum AFP (**E**) in Fra<sup>hep</sup>, c-Jun~Fra<sup>hep</sup> and control mice, after 9-15 months of transgene expression (controls n=32, mutants n=9/11/17/13). **F.** Serum albumin (n=control/mutant: 8/6, 4/5, 7/7) over time in c-Jun~Fra-2<sup>hep</sup> mice and controls. **G.** Serum ALT (left, n=control/mutant: 8/6, 4/5, 7/7), AST (middle, n=control/mutant: 9/13, 5/7, 8/6) and ALP (right, n=control/mutant: 8/6, 4/5, 7/7) over time in c-Jun~Fra-2<sup>hep</sup> mice and controls. **H.** Immunoblot for ER stress-related proteins in liver extracts from c-Jun~Fra-2<sup>hep</sup> mice (non-tumoral and tumors) and controls at 9 months of transgene expression. **I.** IHC for p21 in liver sections from c-Jun~Fra-2<sup>hep</sup> mice and controls. Bar = 100 $\mu$ m, arrows point to positive nuclei. **J.** qRT-PCR quantification of *p21*, *p16*, *p19* and *p53* in c-Jun~Fra-2<sup>hep</sup> livers compared to controls at 2 months. Tubulin is used to control immunoblot loading. Bars = means  $\pm$ SEM. \*  $p < 0.05$ , \*\*  $p < 0.01$ , \*\*\*  $p < 0.001$  (t-test to controls).

### Supplementary Figure 2: Related to Figure 2

**A.** Top enriched cell cycle-related MSigDB Hallmark signatures in mutant RNAseq groups compared to their respective controls (2 months: n=6, 9 months: n=3) by GSEA. Normalized enrichment scores (NES) are shown as bars and FDR q-values ( $-\log_{10}$ ) as dot plots. Data are ordered by NES in the 2 months dataset. **B.** CIBERSORTx deconvolution of hepatocyte subsets in c-Jun~Fra-2<sup>hep</sup> liver RNAseq datasets (control: C, n=6, mutant: NT, n=3) at 2 months. **C.** IHC for Glutamine synthetase (GS) in liver sections from c-Jun~Fra-2<sup>hep</sup> mice and controls at 2 months of transgene expression. Bar = 100 $\mu$ m. **D.** Immunoblot analyses of c-Jun (detecting endogenous

c-Jun and ectopic c-Jun~Fra-2) and various Cyclins and Cdks in liver extracts from c-Jun~Fra-2<sup>hep</sup> mice (non-tumoral and tumors) and controls. **E.** qRT-PCR quantification of *ccna2* (encoding Cyclin A2), *cdk1* and *Il6* expression over time in c-Jun~Fra-2<sup>hep</sup> tumors and non-tumoral (NT) liver areas compared to controls. **F.** IHC quantification of F4/80, Pax5 and CD3 in liver sections of c-Jun~Fra-2<sup>hep</sup> mice and controls at 2 months. **G.** qRT-PCR quantification of immune-cell markers in c-Jun~Fra-2<sup>hep</sup> tumors and non-tumoral (NT) liver areas compared to controls. **H.** Heat map of MSigDB C8 liver cell gene sets (AIZARANI\_LIVER) enriched in each mutant group. Rows display the NES of the 27 gene sets (out of 31) that had FDR>25% in the 3 datasets, grouped by cell type. **I.** Immunoblot analyses of total and phosphorylated ERK, JNK, p38, PTEN, AKT and GSK3 $\beta$  in livers from c-Jun~Fra-2<sup>hep</sup> mice (non-tumoral and tumors) and controls. **J.** IHC for phosphorylated Stat-3 in liver sections from c-Jun~Fra-2<sup>hep</sup> mice and controls at 9 months of transgene expression. Bar = 100 $\mu$ m, arrows point to positive nuclei. **K.** Immunoblot for total and phosphorylated Stat3 in liver extracts from c-Jun~Fra-2<sup>hep</sup> mice and controls at 2 months of transgene expression. Tubulin, Actin and Vinculin are used to control immunoblots loading. Bars = means  $\pm$ SEM, n $\geq$ 3. \* p<0.05, \*\* p<0.01, \*\*\* p<0.001 (t-test to controls).

### Supplementary Figure 3: Related to Figure 3

**A.** qRT-PCR quantification of fibrosis-associated genes in c-Jun~Fra-2<sup>hep</sup> tumors and non-tumoral (NT) liver areas compared to controls. **B.** MSigDB Hallmark signatures for EMT (upregulated) and lipid metabolism (downregulated) in mutant RNAseq groups compared to their respective controls (2 months: n=6, 9 months: n=3) by GSEA. Normalized enrichment scores (NES) are shown as bars and FDR q-values ( $-\log_{10}$ ) as dot plots. Data are ordered by NES in the 2 months dataset. **C.** Immunoblot for Ppar $\gamma$  and Fsp27 in liver extracts from c-Jun~Fra-2<sup>hep</sup> mice and controls at 2 months. **D.** Expression of *pparg2* and selected Ppar $\gamma$  target genes by RNAseq in c-Jun~Fra-2<sup>hep</sup> livers at 2 and 9 months (tumors and non-tumoral), each relative to their respective controls (set to 1). Mean fold change (log<sub>2</sub>) is shown and all changes except one (indicated by \$) are

statistically significant after multiple testing corrections. The red dotted line marks the 2-fold change threshold. **E.** Expression of *nr1h3* (encoding LXR $\alpha$ ) *nr1h4* (encoding FXR) and selected LXR $\alpha$  target genes by RNAseq in c-Jun~Fra-2<sup>hep</sup> livers at 2 and 9 months (tumors and non-tumoral). Adjusted p value is plotted against mean fold change (log<sub>2</sub>) for each sample group relative to its control group. The red dotted line marks the 0.05 p value cut-off and the 2 vertical dotted lines mark the 2-fold change thresholds. **F.** Serum triglycerides (TG, n=4/4) and cholesterol (COL, n=7/7) in c-Jun~Fra-2<sup>hep</sup> mice and controls at 9 months. SP1 is used to control immunoblots loading. Bars = means  $\pm$ SEM, n $\geq$ 3. \* p<0.05, \*\* p<0.01, \*\*\* p<0.001 (t-test to controls).

#### Supplementary Figure 4: Related to Figure 4

**A.** c-Myc IHC (top, bar = 100 $\mu$ m, arrows point to positive nuclei) and immunoblot (bottom) in liver sections or extracts from c-Jun~Fra-2<sup>hep</sup> mice and controls at 2 months. **B.** qRT-PCR quantification of *c-myc* expression in Fra<sup>hep</sup> (n=3) and c-Jun~Fra<sup>hep</sup> (n=3) livers compared to controls (n=12) at 2 months. **C.** qRT-PCR quantification of *foxm1* expression over time in c-Jun~Fra-2<sup>hep</sup> tumors and non-tumoral (NT) liver areas compared to controls. **D.** qRT-PCR analyses of *c-jun*, *fra-2* and *c-myc* in livers from 4 weeks-old mice lacking *fra-2* expression in the liver (Fra-2<sup>Ali</sup>) and Fra-2-proficient control littermates, 48hrs after diethylnitrosamine (DEN) injection. For each gene, expression is plotted relative to mean expression in 2 untreated controls (set to 1, dotted line). **E.** Representative liver morphology (left) and mean surface nodules quantification (right) in Fra-2<sup>Ali</sup> and control mice 9 months post-DEN (injected at 2 weeks of age). Bar = 1 cm, tumors are indicated by arrows. **F.** Serum AFP and ALT in Fra-2<sup>Ali</sup> and control mice 9 months after DEN. **G.** qRT-PCR analysis of *c-jun*, *fra-2* and *c-myc* in liver tumors from Fra-2<sup>Ali</sup> and control mice 9 months after DEN. For each gene, expression is plotted relative to mean expression in 3 untreated controls (set to 1, dotted line). **H.** Data mining using publicly available human liver-related ChIP-seq datasets: JUN, FRA2 and p300 ChIP-seq peak distribution around the c-MYC gene in human HepG2 liver cells. The red dotted box indicates the conserved c-Myc 3' enhancer

(WRE) enhancer. **I.** MYC expression in HepG2 cells either wild-type or with CRISPR knock-out of the c-MYC (WRE) enhancer after transient expression of GFP with increasing amounts of c-Jun~Fra-2 expression vectors (n=2 per point). qRT-PCR values are plotted as a ratio to GFP with MYC expression in HepG2 cells expressing only GFP set to 1. **J.** MYC qRT-PCR in HepG2 cells after siRNA knock-down of JUN genes relative to cells treated with scrambled (scr) siRNA. **K.** Correlation plots for JUN, FRA2 and MYC mRNA expression in human HCC patients using publicly available (TCGA) datasets (n=365). Fragments Per Kilobase of transcript per Million mapped reads (FPKM) are plotted. In the plot on the right side, samples with high JUN and FRA2 (HH, n=136) or low JUN and FRA2 (LL, n=99) are shown in red and grey, respectively (cut off = 30.55 for Jun and 4.03 for FRA2). **L.** MYC, FOXM1 and CCND1 (encoding for Cyclin D1) expression in HH and LL patients (Mann-Whitney test). **M.** TCGA score stratification of Overall Survival comparing HH to LL patients ( $p$  by Mantel-Cox Log-rank test). Tubulin is used to control immunoblot loading. Bars/dots = means  $\pm$ SEM. \*  $p < 0.05$ , \*\*  $p < 0.01$ , \*\*\*  $p < 0.001$  (t-test to controls).

### Supplementary Figure 5: related to Figure 5

**A.** Liver to body weight (left) ratio and Serum ALT (right) at endpoint in un-reverted (9 months ON) and reverted (OFF, 9 months ON then 6 months OFF) c-Jun~Fra-2<sup>hep</sup> and control mice. Reversion escapers are marked in red. **B.** Serum AFP over time in 6 mutants subjected to the reversion protocol and longitudinal US monitoring. **C.** qRT-PCR quantification of c-Jun~Fra-2 in liver samples (tumoral and non-tumoral) from c-Jun~Fra-2<sup>hep</sup> mice at the OFF endpoint compared to non-tumoral (NT) liver areas and tumors (set to 1) from un-reverted (ON) c-Jun~Fra-2<sup>hep</sup> mice. **D.** c-Myc and c-Fos IHC in liver sections or extracts from c-Jun~Fra-2<sup>hep</sup> mice and controls at endpoint of the reversion protocol. Arrows point to positive nuclei. Bar = 100 $\mu$ m. **E.** qRT-PCR quantification of a selection of c-Myc target genes in tumors and non-tumoral (NT) liver areas from c-Jun~Fra-2<sup>hep</sup> mice either un-reverted (ON) or with tumors that escaped reversion (OFF) relative to (pooled) controls. **F.** qRT-PCR for *fos* in tumors (T) and non-tumoral (NT) liver areas from un-

reverted (ON) and reverted (OFF) c-Jun~Fra-2<sup>hep</sup> mice compared to controls. Mice with reversion escapers are plotted separately (red). **G.** qRT-PCR quantification of *c-myc* and c-Myc target genes in the livers of in Fos<sup>hep</sup> mice livers compared to controls at 2 months,  $p < 0.05$  for each mRNA. Bars/dots = means  $\pm$ SEM. \*  $p < 0.05$ , \*\*  $p < 0.01$ , \*\*\*  $p < 0.001$  (t-test).

### Supplementary Figure 6: related to Figure 6

**A.** Experimental design and timeline of the therapeutic trials. US: Ultrasonography. **B-E.** c-Jun~Fra-2<sup>hep</sup> mutants with 2 months of transgene expression (off Dox at weaning) were randomized and treated with JQ1 or vehicle (VEH, during 4 weeks. **B.** Flag IHC in liver sections from c-Jun~Fra-2<sup>hep</sup> mice treated with JQ1 or VEH compared to controls. Bar = 100 $\mu$ m. **C.** qRT-PCR for c-Myc & c-Myc target genes in livers from c-Jun~Fra-2<sup>hep</sup> mice treated with JQ1 or VEH compared to VEH-treated controls.  $p < 0.05$  between VEH-treated mutants and controls for all genes. Serum AFP (**D**), ALT, AST and ALP (**E**), in c-Jun~Fra-2<sup>hep</sup> mice 2 months after transgene induction (start) and after 4 weeks of JQ1 or VEH treatment. 3 VEH-treated and at least 3 untreated control mice are included as healthy reference. **F.** IHC quantification of Ki67 in hepatocytes (hep) and immune cells and of Cyclin D1 and  $\gamma$ H2AX in hepatocytes using liver sections of VEH-treated controls and VEH or JQ1-treated c-Jun~Fra-2<sup>hep</sup> mice. **G.** Serum ALT, AST and ALP at start and endpoint in c-Jun~Fra-2<sup>hep</sup> mutants with 9 months of transgene expression (off Dox at weaning) and treated with JQ1 or VEH during 2 months. 2 VEH-treated control mice are included as healthy reference. **H.** qRT-PCR quantification of immune- and fibrosis-related genes at endpoint in liver samples comparing VEH- and JQ1-treated (responsive) c-Jun~Fra-2<sup>hep</sup> mice. Bars = means  $\pm$ SEM. In dot plots and graphs, means  $\pm$ SEM are plotted. \*:  $p < 0.05$ , \*\*  $p < 0.01$ , \*\*\*  $p < 0.001$  (t-test).

### Supplementary Figure 7: related to Methods

**A.** Liver morphology, histology (H&E, middle) and Flag IHC (bottom) in a c-Jun~Fra-1<sup>hep</sup> and control mouse. Bar = 1 cm (top) and 100 $\mu$ m (middle and bottom). **B.** Immunoblot analyses of c-

Jun (detecting endogenous c-Jun and ectopic c-Jun~Fra-1) in liver extracts from c-Jun~Fra-1<sup>hep</sup> mice and controls at 5 months. **C.** qRT-PCR quantification of *pparg2*, *fra-2*, *p21*, *p16*, *ccnd1* (encoding Cyclin D2) and *ccna2* (encoding Cyclin A2) in c-Jun~Fra-2<sup>hep</sup> livers compared to controls at 2 months. Vinculin is used to control immunoblot loading. **C.** Liver/body weight ratio over time in c-Jun~Fra-1<sup>hep</sup> mice and controls. **D.** Serum cholesterol (left) and triglycerides (right) over time in c-Jun~Fra-1<sup>hep</sup> mice and controls. **F.** Liver triglycerides content in c-Jun~Fra-1<sup>hep</sup> mice and controls at 9 months. **G.** Serum ALT (left) and ALP (right) over time in c-Jun~Fra-1<sup>hep</sup> mice and controls. **H.** Serum ALT, AST and ALP in c-Jun~Fra-1<sup>hep</sup> mice and controls at 12 months.

### **Supplementary Table 1: related to Figure 5**

Summary of ultrasound and blood parameters at start and endpoint in **(A)** 6 mutants and 2 controls subjected to the reversion protocol with blood and ultrasound follow up depicted in Figure 5. Neo-tumors are indicated with an asterisk. **(B)** 6 mutants treated with either JQ-1 or vehicle with blood and ultrasound follow up depicted in Sup Figure 6. Neo-tumors in VEH-treated mutants are indicated with an asterisk and tumor burden values at end point include these tumors.

### **Supplementary Table 2: related to Methods**

Primers used in the study.

### **Supplementary Table 3: related to Methods**

Antibodies used in the study.

### **Supplementary Materials and Methods**

#### *Mice and treatments*

Jun~Fra-2<sup>hep</sup>, Fra-1<sup>hep</sup>, Fra-2<sup>hep</sup>, Fos<sup>hep</sup>, Fra-2<sup>Ali</sup> mice were previously described (1-3). The tet-switchable Col1a1::TetOP-Jun~Fosl1 allele, that was combined to the LAP-tTA allele (MGI:3056818) to generate Jun~Fra-1<sup>hep</sup> mice, was generated with the CNIO Mouse Genome

Editing Core Unit according to (4) and similar to the other tet-switchable AP-1 alleles (MGI:5586533, MGI:5585716, MGI:5585642, MGI:5555845) used in this study. Additional data related to the analysis of Jun~Fra-1<sup>hep</sup> mice can be found in [Suppl. Figure 7](#). Mice were backcrossed and maintained on pure C57BL/6J background and male mice were used for all experiments. Liver samples from c-Jun<sup>Ali</sup>; HBV<sup>tg</sup> mice used in this study were generated in a previously published study (5). Randomized block design was used to organize the experimental cohorts and littermates used as controls. Mice were housed in Specific Pathogen-Free environment with free access to food and drink. Dox (1g/l, Sigma-Aldrich) was supplied in sucrose-containing (100g/l) drinking water to breeding cages and experimental cohorts weaned on normal drinking water (OFF dox). 2 week-old pups or 8 week-old mice were injected intraperitoneally with 25 or 100 mg/kg DEN (Sigma-Aldrich) and sacrificed 9 months or 48 hours after DEN injection, respectively. JQ-1 (Abmole, M2167) was dissolved in 10% (2-Hydroxypropyl)- $\beta$ -cyclodextrin (Abmole, M4893) and mice received a daily dose of 25mg/kg or an equal volume of vehicle by intraperitoneal injection. Sorafenib (Abmole, M3026) was dissolved in a 1:1 mixture of 95% ethanol and Cremophor EL (Sigma, 238470-1SET) and mice received a daily dose of 10mg/kg or an equal volume of vehicle by oral gavage. Liver tumors were detected and measured longitudinally by the CNIO imaging unit with a micro-ultrasound system (Vevo 770, Visualsonics) and an ultrasound transducer of 40 MHz (RMV704, Visualsonics). Mice were anesthetized with a continuous flow of 1% to 3% isoflurane in 100% oxygen at a rate of 1.5 liter/min on a heated bed to prevent hypothermia and abdominal hair was removed using a depilatory cream. Tumor size was calculated as  $\frac{4}{3}\pi x A x B x C$ , where A, B, and C are the lengths of the three semi-axes of the tumor. All animal experiments were performed in accordance with institutional, national, and European guidelines for animals used in biomedical research and approved by the Spanish National Cancer Research Centre (CNIO) Institutional Animal Care and Use Committee and the CNIO–Instituto de Salud Carlos III Ethics Committee for Research and Animal Welfare and the

Austrian Federal Ministry of Education, Science and Research (approved project Wagner E. 171/18).

#### *Blood and liver chemistry analyses*

Blood was collected by submandibular vein or cardiac (experimental endpoint) puncture. Routine blood measurements were performed using a VetScan (Abaxis) or a Reflovet Plus (Scil Diagnostics) blood chemistry analysers. AFP & PIVKA were measured on serum samples by ELISA (R&D, MAFP00 and FineTest, EM1857, respectively). For liver Triglyceride content, 25-75mg of liver tissue was homogenized in chloroform/methanol (8:1 v/v; 500ul per 25 mg tissue) and shaken at RT for 8-16 hours. H<sub>2</sub>SO<sub>4</sub> was added to a final concentration of 0.28M and the lower phase collected after centrifugation, dried, and Triglycerides measured using an enzymatic assay kit (Cayman Chemicals, 10010303).

#### *Histology*

Tissues were frozen in OCT (Tissue-tek) or fixed in 4% formalin and embedded in paraffin and 4µm sections prepared. Standard procedures were used for H&E-, Masson's trichrome and Oil-red-O stainings. IHC was performed either by the CNIO Histopathology Core Unit or manually as previously described (1, 3) using matching secondary antibodies from the Vectastain Elite ABC kits (Vector Laboratories) and Carazzi's hematoxylin (Panreac AppliChem) counterstaining. Quantification was performed on digital scans using Panoramic Viewer (3DHistech) and ImageJ softwares. Antibodies are listed in [Suppl. Table 3](#).

#### *Protein isolation, Immunoblot and Chromatin immunoprecipitation*

Small pieces of fresh or snap frozen livers were disrupted using a Precellys device (Bertin Technologies) in RIPA buffer (50 mM Tris, pH 7.4, 150 mM NaCl, 1% NP-40, 0.5% Na-deoxycholate, and 0.1% SDS). Protein lysates were quantified using a BCA protein assay reagent (Thermo Fisher Scientific). Immunoblot analysis was performed using standard protocols as

described (2, 3). Chromatin immunoprecipitation (ChIP) on murine liver samples was performed as detailed in (2) and quantitative PCR (qPCR) was used to quantify amplified fragments using GoTaq qPCR Master Mix (Promega) and Eppendorf fluorescence thermocyclers with duplicate reactions. The  $2^{\Delta\Delta CT}$  method was used to quantify amplified fragments in the Input and ChIP fractions and calculate input recovery in each condition. ChIP-qPCR primers and ChIP antibodies are listed in [Suppl. Table 2](#) and [Suppl. Table 3](#), respectively.

#### *Cell culture and in vitro experiments*

Murine AML12 and human HepG2 liver-derived cell lines were maintained in DMEM supplemented with 10% FBS at 37°C and 5% CO<sub>2</sub>. To delete the c-MYC (WRE) enhancer, two flanking CRISPR guides were designed (sg\_1: GCCCCTTTGTGGCCTAGGGC and sg\_2: GCCCTAGGCCACAAAGGGGC) and cloned into the lentiCRISPR v2 backbone containing a puromycin selection cassette (Addgene#52961) and the resulting plasmid transfected in HepG2 cells using Xtreme gene (Sigma). Cells underwent selection for 48 hours before isolation and expansion of single clones. CRISPR-edited clones were identified by genotyping PCR (primers: For: TTGGCACGTCATAT and Rev: GAGCTTGGCTATGGG) and deletion of the CRISPR-targeted region confirmed by sequencing. Guides and genotyping primer sequences can be found in [Suppl. Table 2](#). AML12 cells ( $1.25 \times 10^5$  cells/well in a 24 well plate) were transfected in technical quadruplicates using Lipofectamine 2000 (Invitrogen) with 0.05µg Renilla vector (pHRG-tk, Promega), 0.5µg c-Myc 3'enhancer luciferase reporter (6) and 1µg of pBabe-Fra-2, pBabe-Jun~Fra-2, or empty pBabe (control) expression vectors (7). Luciferase activity was measured 48 hours later using the Dual-Glo Luciferase Assay (Promega) and a Szabo Scandic luminometer following the manufacturer's recommendations. AML12 cells ( $3 \times 10^5$  cells/well in a 6 well plate) were transfected in technical duplicates using Lipofectamine 2000 (Invitrogen) with 1µg of pBabe-Fra-2, pBabe-Jun~Fra-2, or empty pBabe (control) expression vectors and cells harvested for RNA preparation and endogenous *c-myc* qRT-PCR 72 hours later. HepG2 cells ( $0.75 \times 10^5$

cells/well in a 24 well plate) were transfected using ON-TARGETplus JUN, JUNB and JUND or scramble siRNAs (Dharmacon) and Lipofectamine RNAiMAX (Thermofisher) transfection reagent and cells harvested 72 hours later for RNA preparation and endogenous MYC and RPL29 (housekeeping) qRT-PCR. Wild-type and c-MYC (WRE) CRISPR-KO HepG2 cells ( $1 \times 10^5$  cells/well in a 24 well plate) were transfected in technical duplicates using Lipofectamine 2000 (Invitrogen) with 0.025  $\mu$ g of pBabe-GFP, 0, 0.25, 0.5 or 1  $\mu$ g of pBabe-Jun~Fra-2 and 1, 0.5, 0.75 or 0  $\mu$ g of empty pBabe (control) expression vectors (1.025  $\mu$ g total DNA per well) and cells harvested 48 hours later for RNA preparation and qRT-PCR for GFP, to adjust for transfection efficiency between all wells, RPL29 (housekeeping) and endogenous MYC. Primer sequences can be found in [Suppl. Table 2](#).

#### *RNA isolation and quantitative reverse transcription-PCR (qRT-PCR)*

Total RNA was isolated using TRI Reagent (Sigma-Aldrich), complementary DNA was synthesized using Ready-To-Go-You-Prime-First-Strand Beads (GE Healthcare) or GoScript™ Reverse Transcription Mix, Oligo(dT) (Promega) and quantitative PCR was performed using GoTaq qPCR Master Mix (Promega) and Eppendorf fluorescence thermocyclers with duplicate reactions and two housekeeping genes (Rpl4 and Rps29) per run. The  $2^{-\Delta\Delta CT}$  method was used to quantify amplified fragments. Primer sequences can be found in [Suppl. Table 2](#).

#### *Bulk RNA-seq, data analysis and datamining*

RNA integrity of total RNA isolated using TRI Reagent (Sigma-Aldrich) was evaluated using an Agilent 2100 Bioanalyzer (Agilent Technologies) and samples with integrity score >8 were used for bulk RNA-seq. RNA processing was performed using TruSeq RNA Sample Preparation kit (Illumina, 15031047) at the CNIO Genomic Core Unit. The resulting purified cDNA library was applied to an Illumina flow cell for cluster generation (TruSeq cluster generation kit v5) according to the manufacturer's protocols and sequenced on an Illumina HiSeq2000 instrument at the Vienna BioCenter Core Facilities NGS Unit. RNA-seq reads (average 24 million reads per sample)

were converted from .bam to .fastq format using bedtools v2.27.1 (8) at the MUV Genomics Core Facility. Reads in fastq format were aligned to the mouse reference genome (GRCm38/mm10) with Gencode mV23 annotations using STAR aligner (9) version 2.6.1a in 2-pass mode. Raw reads per gene were counted by STAR. TPM were generated by RSEM (10). Differential gene expression was calculated using DESeq2 (11) version 1.22.2 with Benjamini-Hochberg adjusted p-values. Differentially expressed genes ( $1 < \log_2\text{foldchange} < -1$ ) with an adjusted P value of  $< 0.05$  were considered statistically significant. RNA-seq datasets are deposited in NCBI's Gene expression omnibus archive Omnibus and are accessible through GEO Series accession no. GSE261005. Differentially expressed genes were explored by Gene Set Enrichment Analysis (GSEA) (12) using the GSEA software and gene sets downloaded from the Molecular Signature Database ([www.gsea-msigdb.org/gsea/msigdb/](http://www.gsea-msigdb.org/gsea/msigdb/)). P-values and the false discovery rate (FDR) for the enrichment score of each gene set were calculated based on 1000 gene set permutations and statistical significance (nominal P value) of the Enrichment Score calculated using an empirical phenotype-based permutation test. Over-representation (ORA) analysis was conducted on WebGestalt (13) by uploading differentially expressed gene lists to the web server (<http://www.webgestalt.org>) and selecting Pathways/Reactome and Gene Ontology/Biological processes as Method/Functional database for analyses with advanced parameters set to default. Enriched categories were ranked based on FDR and then the top 7 most significant categories selected for plotting. Published murine hepatocyte and myeloid single cell reference matrix files (14) were retrieved and uploaded to the CIBERSORTx webserver ([www.cibersortx.stanford.edu/](http://www.cibersortx.stanford.edu/)), together with raw gene expression counts from individual bulk RNA-Seq datasets prepared following CIBERSORTx (15) guidelines. The Impute Cell Fractions module was utilized to estimate cell type abundancies in individual samples from each dataset with Absolute mode, S-mode batch correction, 500 Permutations and Disable quantile normalization options checked. Genome-wide of HepG2 hepatoma cells (16) ChIP-seq datamining was performed using the ENCODE portal ([www.encodeproject.org](http://www.encodeproject.org)) and ChIP-seq traces around the c-MYC gene retrieved

from experiments ENCSR000EEK, ENCSR000BHP and ENCSR000BLW corresponding to ChIP for JUN, FRA2 and P300, respectively. The TCGA-LIHC Cancer Genome Atlas (17) treatment-naïve HCC patients clinical data (OS) and the corresponding JUN, FRA2, MYC, FOXM1 and CCND1 normalized RNAseq data from surgical resection specimens were retrieved from the Human Protein Atlas Portal ([www.proteinatlas.org/](http://www.proteinatlas.org/)).

### Statistics

Methods for statistical evaluation of RNA-seq data are indicated above. For the rest of the data and unless otherwise specified, data in plots and bar graphs are presented as mean  $\pm$  SD and statistical significance determined using unpaired two-tailed Student's t test, except for Kaplan–Meier plots where Mantel–Cox log-rank was used, values of  $P < 0.05$  were considered statistically significant.

### Supplementary References (related to Methods)

1. S. C. Hasenfuss, L. Bakiri, M. K. Thomsen, R. Hamacher, E. F. Wagner, Activator Protein 1 transcription factor Fos-related antigen 1 (Fra-1) is dispensable for murine liver fibrosis, but modulates xenobiotic metabolism. *Hepatology* **59**, 261-273 (2014).
2. S. C. Hasenfuss *et al.*, Regulation of steatohepatitis and PPARgamma signaling by distinct AP-1 dimers. *Cell Metab* **19**, 84-95 (2014).
3. L. Bakiri *et al.*, Liver carcinogenesis by FOS-dependent inflammation and cholesterol dysregulation. *J Exp Med* **214**, 1387-1409 (2017).
4. C. Beard, K. Hochedlinger, K. Plath, A. Wutz, R. Jaenisch, Efficient method to generate single-copy transgenic mice by site-specific integration in embryonic stem cells. *Genesis* **44**, 23-28 (2006).
5. C. Trierweiler *et al.*, The transcription factor c-JUN/AP-1 promotes HBV-related liver tumorigenesis in mice. *Cell Death Differ* **23**, 576-582 (2016).
6. G. S. Yochum, R. Cleland, R. H. Goodman, A genome-wide screen for beta-catenin binding sites identifies a downstream enhancer element that controls c-Myc gene expression. *Mol Cell Biol* **28**, 7368-7379 (2008).
7. L. Bakiri, K. Matsuo, M. Wisniewska, E. F. Wagner, M. Yaniv, Promoter specificity and biological activity of tethered AP-1 dimers. *Mol Cell Biol* **22**, 4952-4964 (2002).
8. A. R. Quinlan, I. M. Hall, BEDTools: a flexible suite of utilities for comparing genomic features. *Bioinformatics* **26**, 841-842 (2010).
9. A. Dobin *et al.*, STAR: ultrafast universal RNA-seq aligner. *Bioinformatics* **29**, 15-21 (2013).
10. B. Li, C. N. Dewey, RSEM: accurate transcript quantification from RNA-Seq data with or without a reference genome. *BMC Bioinformatics* **12**, 323 (2011).
11. M. I. Love, W. Huber, S. Anders, Moderated estimation of fold change and dispersion for

- RNA-seq data with DESeq2. *Genome Biol* **15**, 550 (2014).
12. A. Subramanian *et al.*, Gene set enrichment analysis: a knowledge-based approach for interpreting genome-wide expression profiles. *Proc Natl Acad Sci U S A* **102**, 15545-15550 (2005).
  13. Y. Liao, J. Wang, E. J. Jaehnig, Z. Shi, B. Zhang, WebGestalt 2019: gene set analysis toolkit with revamped UIs and APIs. *Nucleic Acids Res* **47**, W199-W205 (2019).
  14. R. Carlessi *et al.*, Single-nucleus RNA sequencing of pre-malignant liver reveals disease-associated hepatocyte state with HCC prognostic potential. *Cell Genom* **3**, 100301 (2023).
  15. A. M. Newman *et al.*, Determining cell type abundance and expression from bulk tissues with digital cytometry. *Nat Biotechnol* **37**, 773-782 (2019).
  16. E. C. Partridge *et al.*, Occupancy maps of 208 chromatin-associated proteins in one human cell type. *Nature* **583**, 720-728 (2020).
  17. C. G. A. R. Network., Comprehensive and Integrative Genomic Characterization of Hepatocellular Carcinoma. *Cell* **169**, 1327-1341 e1323 (2017).